Author Manuscript

Author Manuscript

Author Manuscript

Author Manuscript

HHS Public Access

Author manuscript

Nano Today. Author manuscript; available in PMC 2017 June 01.

Published in final edited form as:

Nano Today. 2016 June ; 11(3): 309–329. doi:10.1016/j.nantod.2016.05.010.

Fluorescent nanoprobes for sensing and imaging of metal ions: recent advances and future perspectives

JingJing Zhang[1], **FangFang Cheng**[2], **JingJing Li**[2], **Jun-Jie Zhu**[2], and **Yi Lu**[1]

[1]Department of Chemistry, University of Illinois at Urbana-Champaign, Urbana, IL 61801, USA

[2]College of Chemistry, Nanjing University, Nanjing, P. R. China.

Summary

Recent advances in nanoscale science and technology have generated nanomaterials with unique optical properties. Over the past decade, numerous fluorescent nanoprobes have been developed for highly sensitive and selective sensing and imaging of metal ions, both *in vitro* and *in vivo*. In this review, we provide an overview of the recent development of the design and optical properties of the different classes of fluorescent nanoprobes based on noble metal nanomaterials, upconversion nanoparticles, semiconductor quantum dots, and carbon-based nanomaterials. We further detail their application in the detection and quantification of metal ions for environmental monitoring, food safety, medical diagnostics, as well as their use in biomedical imaging in living cells and animals.

Graphical Abstract

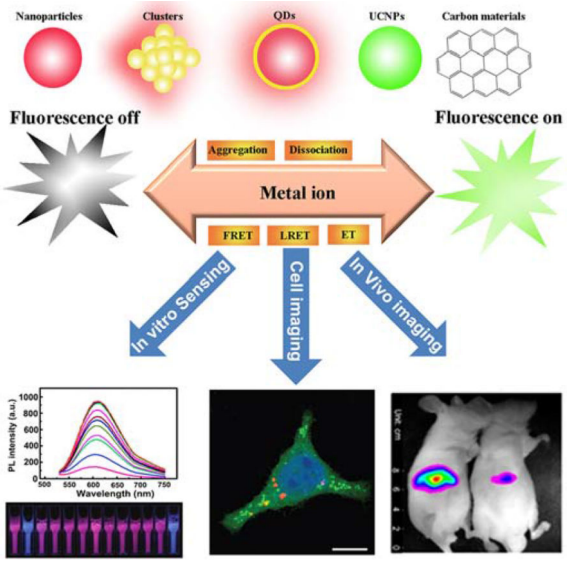

Corresponding author: Prof Yi Lu, yi-lu@illinois.edu.

Publisher's Disclaimer: This is a PDF file of an unedited manuscript that has been accepted for publication. As a service to our customers we are providing this early version of the manuscript. The manuscript will undergo copyediting, typesetting, and review of the resulting proof before it is published in its final citable form. Please note that during the production process errors may be discovered which could affect the content, and all legal disclaimers that apply to the journal pertain.

Author Manuscript Author Manuscript Author Manuscript Author Manuscript

Keywords

Fluorescent nanoprobes; Metal ions; Noble metal; Upconversion nanoparticles; Quantum dots; Carbon nanomaterials

INTRODUCTION

Metal ions play fundamental roles in biology by serving as essential cofactors in processes such as energy metabolism and storage, signal transduction, and nucleic acid processing [1-7]. However, some essential metals ions, including Fe^{2+}, Cu^{2+}, Mn^{2+}, and Co^{2+}, can also be toxic at high doses [8]. Therefore, metal import, trafficking, availability, and export must be tightly regulated at the cellular level. In addition, other heavy metal ions, such as Hg^{2+}, Cd^{2+}, Pb^{2+}, and As^{3+}, are acutely toxic to humans and aquatic species even at low concentrations, and bioaccumulation of these metal ions can cause serious health problems [9]. Therefore, developing selective and sensitive methods to detect and quantify metal ions for environmental monitoring, food safety, and medical diagnostics and imaging is of considerable importance.

Traditional analytical techniques for metal ion detection, such as atomic absorption or emission spectroscopy (AAS/AES) [10], inductively coupled plasma mass spectrometry (ICP-MS) [11], anodic stripping voltammetry [12], and capillary electrophoresis [13], typically require expensive instrumentation and/or complicated sample preparation, making it difficult for on-site and real-time detection. In light of these drawbacks, there is increasing interest in developing new sensing techniques for the detection of metal ions that have higher sensitivity and selectivity, shorter response times, and lower costs [14]. Among the current sensor approaches, fluorescence detection [3,15-21] is the most common analytical tool used in the detection of metal ions due to its capabilities for sensitivity, selectivity, reproducibility, and rapid, real-time monitoring. The critical element that achieves this goal is the fluorescent probe which offers a real-time, noninvasive way to image metal ions in their native environments with high spatial and temporal resolution [3]. Because of these capabilities, fluorescent probes have contributed greatly to insights into production, localization, trafficking, and biological roles of metal ions in complex living systems [3,19].

Organic dyes, such as rhodamine, fluorescein, and cyanine, are the most commonly used fluorescent probes [22-24], but their low absorption coefficients and weak signal reduce the sensitivity and response of metal ions [5,25-27]. In addition, most organic fluorophores undergo irreversible photobleaching during prolonged illumination, which makes them incapable of continuous observation and long-term imaging for studies of living cells [28]. Furthermore, some organic dyes, such as fluorescein isothiocyanate (FITC), are strongly phototoxic, and could produce reactive oxygen species (ROS) in the excitation process. These drawbacks have stimulated the development of alternative fluorescent probes for metal ions with brighter luminescence, higher photostability, and better biocompatibility, through advances in the fields of nanoscale science and engineering. The typical construction of fluorescent nanoprobes starts with synthesis of the nanoprobes using top-down or bottom-up approaches, followed by designed surface modifications. The precisely-

Author Manuscript Author Manuscript Author Manuscript Author Manuscript

controlled preparation of size, shape, chemical composition, and surface chemistry of the nanoprobes is critical to obtain unique optical properties and high performance in sensing and imaging applications.

Recent advances in nanobiotechnologies are expanding the availability of nanomaterials varying in size and structure [29-32], offering many exciting opportunities for discovering new fluorescent nanoprobes [33-39]. A variety of nanoprobes have already been prepared, evaluated, and applied in fluorescent sensing and imaging of various metal ions, including metal nanomaterials [40-42], lanthanide-doped upconversion nanoparticles (UCNPs) [43-47], semiconductor quantum dots (QDs) [48,49], and carbon-based nanomaterials [50-54]. These fluorescent nanoprobes can overcome several limitations of conventional organic dyes, such as poor hydrophilicity and photostability, low quantum yield and detection sensitivity, insufficient stability in biological systems, and weak multiplexing capability [55,56]. In addition, surface functionalization of these nanomaterials offers selective delivery of the nanoprobes to specific cells or even to subcellular organelles to realize effective intracellular imaging.

Several excellent review papers have been published to highlight the potential of fluorescent nanoprobes for analyzing metal ions in environmental and biological samples [57-62]. However, most of the reviews focused on either environmental sensing or biological imaging. In an effort to fill this gap, we herein review the literature of the last five years covering recent advances of different fluorescent nanoprobes in both sensing and imaging systems for metal ions. The representative literature reports utilizing fluorescent nanoprobes for metal ion sensing are summarized in Table 1. Current challenges and future prospects of fluorescent nanoprobes for fundamental studies and clinical applications will also be discussed.

2. Noble metal nanomaterials-based fluorescent nanoprobes for sensing and imaging of metal ions

Noble metal nanomaterials, such as gold and silver, have frequently been used in the construction of fluorescent nanoprobes for metal ions during the past decade because of their unique optical properties [63-65]. These metal nanomaterials can be categorized into two types based on the size and optical properties: colloid metal nanoparticles (NPs) and metal nanoclusters (NCs). Colloid metal NPs generally refer to materials with diameters more than 10 nm and less than a few hundred nm. Typically, these NPs produce localized surface plasmon resonance (LSPR) and strong light scattering [66-69], however, they usually have poor intrinsic fluorescent quantum yields (QYs) that are not suitable for direct fluorescent sensing of metal ions. Nevertheless, with the ability to quench molecular excited states, colloid metal NPs could function as effective photoluminescence (PL) quenchers in designing fluorescence-based sensors. On the other hand, metal NCs are defined as small metal clusters (e.g., Au, Ag, Cu, and Pt) with size ranges from sub-nanometer to 10 nm in diameter. Specific features of such metal NCs include high fluorescence, excellent photophysical and chemical stability, good biocompatibility, controllable sizes and tunable emissions, and rich surface chemistry for functionalization [70]. Because of these useful

Author Manuscript Author Manuscript Author Manuscript Author Manuscript

features, fluorescent probes using metal NCs have contributed to the development of many innovative analytical methods for biosensing and bioimaging *in vitro* and *in vivo*.

2.1 Colloid metal nanoparticles

2.1.1 Detection of metal ions in environmental and biological samples—Colloid metal NPs with unique optical properties have been widely used for the detection of metal ions in environmental and biological samples [71]. Among these, gold nanoparticles (AuNPs), including nanospheres and nanorods, are especially attractive because of their convenient synthesis, biocompatibility, and novel optical properties. The synthesis of AuNPs can date back to Michael Faraday's work in 1857, in which the gold hydrosols were prepared by reduction of an aqueous solution of chloroaurate with phosphorus dissolved in carbon disulfide. Since then, numerous methods have been developed to synthesize and functionalize AuNPs, and these methods have been extensively reviewed in the past [72-74]. Although AuNPs display rather weak fluorescence, they can be used in fluorescent sensors as a "super-quencher" for almost all dyes, because the quenching effect of AuNPs is generally several orders of magnitude higher than that of an organic quencher. Therefore, a critical parameter for fluorescent sensing using AuNPs is the change in distance between the fluorophore and AuNP. This sensing can be achieved by linking a fluorophore probe with a target recognition molecule conjugated to the AuNP. Following this principle, AuNPs have been successfully used to construct fluorophore and quencher-based biosensors for a broad range of metal ions [75].

Among the many classes of molecules utilized as metal recognition elements, organic complexes are one of the most widely used, due to the diversity in their structural types and physico-chemical characteristics for intramolecular charge transfer (ICT). As an example, Wang et al. [76] reported a turn-on fluorescent sensor for the detection of Pb^{2+} in wastewater samples using a fluorophore–AuNP assembly (Figure 1A). A fluorescent organic complex, brilliant cresyl blue (BCB), was assembled on negatively charged glutathione (GSH)-modified AuNPs via electrostatic interaction, resulting in fluorescence quenching of the fluorophore. In the presence of Pb^{2+}, fluorescent BCB molecules were detached from AuNPs due to the formation of a chelating complex between Pb^{2+} and GSH confined on AuNPs, restoring the BCB fluorescence. The limit of detection (LOD) was 0.51 nM, and the potential coexisting ions (e.g. Al^{3+}, Ca^{2+}, Co^{2+}, Cr^{2+}, Cu^{2+}, Cd^{2+}, K^{+}, Na^{+}, Mg^{2+}, Mn^{2+}, Zn^{2+}, Fe^{3+}) induced less than ±5% interference in the detection of Pb^{2+}. Similarly, rod-shaped AuNPs functionalized with bisacridinedione complex were applied for Ca^{2+} detection by Kim and Park Group [77]. In other cases, the same group reported a series of fluorometric chemosensors for selective signaling toward Ca^{2+} and Mg^{2+}, using aza-crown ether acridinedione-functionalized AuNPs as the probes [78,79]. However, these chemosensors cannot differentiate the fluorescent signal from Ca^{2+} and Mg^{2+} due to similar binding events of crown ethers with these two metal ions. Taking advantage of a similar principle, rhodamine-functionalized AuNPs were also employed to develop "turn-on" fluorescent sensors for sensitive detection of Hg^{2+} [80] and Zn^{2+} [81], with a LOD of 0.32 μM and 0.05 mg/L, respectively. A fluorescence resonance energy transfer (FRET) -based "turn-off" sensor for Cu^{2+} has been recently developed using FITC modified AuNPs by Hormozi-Nezhad et al. [82]. Recently, Wu et al. published an even more sensitive method

Author Manuscript Author Manuscript Author Manuscript Author Manuscript

[83]. In their method, AuNPs functionalized with catechin were synthesized, and upon addition of Pb^{2+}, Pb^{2+}–catechin complexes and Pb–Au alloys that formed on the AuNP surfaces allowed the AuNPs to exhibit peroxidase-mimicking catalytic activity, resulting in a strong enhancement in the emission intensity at 588 nm (>100-fold). In spite of substantial progress, AuNP-based probes with high affinity and selectivity for metal ions remains a challenge.

Alternatively, functional DNAs are another class of recognition molecules for metal ion sensing. DNA–metal ion interactions based on either DNA mismatches or DNA G-quadruplexes have been successfully combined with AuNPs for fluorescent detection of Hg^{2+} and K^{+} [84]. Additionally, the use of metal-ion-dependent DNAzymes as the recognition element has helped advance the development of highly selective and sensitive fluorescent nanoprobes for various metal ions. For instance, a Pb^{2+} sensor was developed by attaching fluorophore-labeled 8–17 DNAzymes and substrates to AuNPs [85]. In the presence of Pb^{2+}, the sensor underwent fluorescence enhancement as a result of the increase in fluorophore-AuNP distance upon DNAzyme-catalyzed cleavage of the substrate. Similarly, rod-shaped AuNPs coated with positively charged surfactants acted as binders and quenchers for fluorophore-labeled 8–17 DNAzymes and substrates [86], allowing the detection of Pb^{2+} by fluorescence enhancement (Figure 1B). Another study used a similar design for Cu^{2+} detection using a Cu^{2+}-dependent DNA-cleaving DNAzyme via a AuNP-based FRET assay [87]. Xie et al. [88] developed a triple-channel optical signal (fluorometric, colorimetric, and resonance light scattering) probe for the detection of Hg^{2+} (Figure 1C), based on the different interactions of AuNPs with single-stranded DNA (ssDNA) and double-stranded DNA (dsDNA), the high binding affinity of positively charged acridine orange dye for DNA, and the modulation of the efficiency of energy transfer between fluorescent dyes and AuNPs.

Another advantage of AuNPs is that they have a broad quenching ability for almost all fluorophores, which enables a multiplex detection of several metal ions, e.g. in homogeneous solution by the anchoring of multiple recognition elements on AuNPs [89]. For instance, Kim et al. [90] developed a multiplex sensing method using aptamer/QD conjugates and AuNPs for Hg^{2+}, K^{+}, and adenosine. In this sensor, the fluorescence of QDs was effectively quenched by the AuNPs due to FRET of QDs to AuNPs. In the presence of targets, the QD-conjugated aptamers were detached from AuNPs by target-induced conformational change of aptamers. Consequently, the fluorescence of the QDs was recovered proportional to the target concentration.

In addition to fluorescence quenching, AuNPs could serve as fluorescence anisotropy generators for the attached fluorophores due to their large size in comparison to free fluorophores and DNA. Based on this principle, a fluorescence anisotropy sensor was constructed using DNAzyme-functionalized AuNPs for the detection of Cu^{2+} and Pb^{2+} [91].

AuNPs can also be used to quench the fluorescence of nanocrystals. As an example, Li et al. [92] reported a nanometal surface energy transfer (NSET) based sensor for Hg^{2+} by using DNA-conjugated QDs and AuNPs (Figure 1D). In the presence of Hg^{2+}, the QDs and the AuNPs were brought into close proximity, leading to quenching of the fluorescence

Author Manuscript Author Manuscript Author Manuscript Author Manuscript

emission of the QDs. This nanosensor exhibited a LOD of 0.4 and 1.2 ppb toward Hg^{2+} in the buffer solution and in river water, respectively. Taking advantage of a similar principle, DNA-conjugated UCNPs and AuNPs were also employed to develop "turn-on" fluorescent sensors for sensitive and simultaneous detection of Pb^{2+} and Hg^{2+}. In addition to the above AuNP-based fluorescent nanoprobes, using similar design concepts, silver nanoprisms and bimetallic platinum/AuNPs were also successfully transformed into fluorescent sensors for the selective and sensitive detection of Tb^{3+} [93] and Hg^{2+} [94], respectively.

2.1.2 Imaging of metal ions within cells and in vivo—The detection and imaging of metal ions within cells and animals are of great significance for medical and biological studies. However, compared with the large amount of work on metal ion detection *in vitro* using colloid metal NP-based fluorescent probes, there are only very limited examples of colloid metal NP-based fluorescent sensors for metal-ion detection in living cells. Colloid metal NPs (e.g. AuNPs) can be easily incorporated into living cells by direct uptake or by any transfection mechanism. Likewise, the quantum mechanical effects, such as photoluminescence emission or plasmon resonance in AuNPs can make AuNPs excellent candidates for a different kind of low cytotoxicity intracellular imaging.

A significant advantage of using AuNP-based probes in intracellular imaging is that they can be used as delivery agents to facilitate entry of other material, such as DNA [95] and organic dyes [96,97], into cells. Using this feature to their advantage, the Lu group [95] has recently developed a fluorescent nanoprobe for intracellular UO_2^{2+} imaging. A 13-nm AuNP was used as an agent for efficient cellular delivery of dye-labeled uranyl-specific 39E DNAzyme. The fluorescence of a Cy3 fluorophore modified at the 5' end of the substrate strand was quenched by both the AuNP and by the molecular quencher modified at the 3' end of the substrate strand (Figure 2A). In the presence of UO_2^{2+}, the DNAzyme cleaved the substrate strand, thus releasing the shorter Cy3-labeled product strand and thereby increasing the fluorescence. This sensor was the first DNAzyme-based probe of metal ions in live cells (Figure 2B). In addition, Liu et al. [96] developed a AuNP-based FRET assay for detection of Hg^{2+}. Rhodamine B isothiocyanate (RBITC) was modified on the surface of AuNPs and the fluorescence was quenched by AuNPs (Figure 2C). Due to higher affinity of Hg^{2+} toward isothiocyanate (ITC), binding with ITC induced detachment of RBITC from the AuNP surface, thus triggering a remarkable enhanced fluorescence of RBITC. This sensor has shown high sensitivity in monitoring Hg^{2+} in complex samples, such as in river water and live cells (Figure 2D), with a LOD of 3.8 nM and 10 μM, respectively. Similarly, Lee et al. [97] proposed a Cu^{2+} nanosensor based on its effect on the fluorescence of a boradiazaindacene (BODIPY) fluorophore, while using AuNPs as agents to promote cellular uptake.

Bradley and co-workers [98] recently reported that Pd NPs trapped within polystyrene microspheres can enter cells and mediate a variety of Pd^0-catalysed reactions, such as allylcarbamate cleavage and Suzuki–Miyaura cross-couplings. Cells were loaded with fluorescently labeled Pd^0 microspheres and the intracellular formation of a carbon–carbon cross-coupled product based on Pd^0-mediated synthesis of an anthofluorescein rhodamine-based dye offered the fluorescent Pd^{2+} imaging in HeLa cells (Figure 3).

Author Manuscript Author Manuscript Author Manuscript Author Manuscript

2.2 Metal nanoclusters

Fluorescent metal NCs have emerged as a new class of fluorophores because of several advantageous features [99-102] such as good fluorescence properties and biocompatibility, excellent photostability, sub-nanometer size, and ease of synthesis. The synthesis, biofunctionalization, and applications of metal NCs have been extensively reviewed elsewhere [17,84,103-107]. In the following section, we focus on the recent advances in the application of fluorescent metal NCs in metal ion sensing and imaging areas.

2.2.1 Detection of metal ions in environmental and biological samples—Metal ions, particularly heavy metal ions, have always been a significant threat to human health and the environment. Many sophisticated methods for rapid, sensitive, and selective detection of heavy metal ions, such as Hg^{2+} [108,109], Cu^{2+} [110,111], and Pb^{2+} [112,113], have been developed using metal NC-based fluorescent probes. One example is a “turn off” sensing system developed for the detection of Hg^{2+}, which takes advantage of Hg^{2+}’s ability to form strong metallophilic bonds with the high percentage of Au^{+} or Ag^{+} present on the surface of NCs, leading to efficient fluorescence quenching of NCs. Xie et al. [114] developed a one-pot route of synthesis to prepare fluorescent AuNCs using bovine serum albumin (BSA) as the template. The BSA-AuNCs consisted of 25 gold atoms and gave an intense red emission (640 nm) when excited at 480 nm. A highly selective and ultrasensitive detection of Hg^{2+}, based on fluorescence quenching of Au nanoclusters by the Hg^{2+}-Au^{+} interaction, was then developed with a LOD of 0.1 ppb, which is lower than the maximum contamination level (MCL) (2.0 ppb) of mercury in drinking water defined by the United States Environmental Protection Agency (EPA). In a complementary effort, the Lu group developed a new method for the selective detection of Hg^{2+} that uses lysozyme-stabilized AuNCs as fluorescent probes [115]. In our method, the selective fluorescent quenching of AuNCs by Hg^{2+} was found to originate from gold clusters and not by the lysozyme-Au^{+} complex. Similarly, Wang et al. [116] also developed a method that could be used in the selective determination of Hg^{2+} by developing a facile approach to synthesize red-emitting fluorescent AgNCs using lysozyme as scaffold. Additionally, luminescent Au/Ag NCs coating with various ligands, including peptide [117], glutathione [116], pepsin [109] and other molecules [118-121], were also reported for the highly sensitive and selective detection of Hg^{2+} or CH_3Hg^{+}. In additional to fluorescence quenching detection methods, turn-on fluorescence methods for rapid, easy, and reliable screening of Hg^{2+} were also developed using DNA-protected AgNCs [122,123].

Copper was also detected using fluorescent metal NCs [111]. For instance, Gui et al. [110] reported the synthesis of human serum albumin (HSA)-stabilized fluorescent Au/Ag core/shell NCs for highly sensitive and selective sensing of Cu^{2+} (Figure 4A). The Au/Ag NCs’ photoluminescence (PL) quenching in the presence of Cu^{2+} was ascribed to the reduction of Cu^{2+} to Cu^{+}, and the subsequent interaction between Cu^{+} and Ag (around Au/Ag NCs). Although Hg^{2+} at a higher concentration (e.g. 5 μM) had a potential influence on the Cu^{2+} sensor, this influence could be distinctly differentiated because Hg^{2+}-induced aggregation of HSA-stabilized Au/Ag NCs resulted in PL quenching. Later, Liu et al. [124] proposed a hydrothermal synthesis of polyelectrolyte -stabilized Ag NCs as selective and ultrasensitive

Author Manuscript Author Manuscript Author Manuscript Author Manuscript

indicators for the simultaneous detection of Hg^{2+} and Cu^{2+}, with the addition of ethylenediaminetetraacetate (EDTA) as the masking agent (Figure 4B).

Lead is a highly toxic metal ion that is often encountered in the environment due to its use in batteries, gasoline, and pigments [125]. Fluorescence quenching or enhancing of metal NCs by lead ions have been developed for screening Pb^{2+} in contaminated lake water samples [126,127] and in DMSO [128]. In addition, an aggregation-induced fluorescence quenching strategy based on coordination of ferric ions and dihydroxyphenylalanine-capped AuNCs has also been applied to the detection of Fe^{3+}, with a LOD of 3.5 μM that is close to the MCL (5.4 μM) of Fe^{3+} permitted in drinking water by the U.S. EPA. Similarly, other metal ions, such as Ag^{+} [129,130], Pd^{2+} [129], Co^{2+} [131], Fe^{3+} [132], Al^{3+} [133], Cr^{3+} [134], Cr^{6+} [134], have also been successfully detected using metal NCs in the past five years.

2.2.2 Imaging of metal ions within cells and in vivo—There are many advantages to using fluorescent metal NCs as an imaging agent in cells and *in vivo*, including their unique functionality, ease in conjugation, biocompatibility, large Stoke shift, long lifetime, as well as their photo- and chemical stability [99-102]. A common strategy for intracellular metal ion imaging is based on the analyte-specific quenching of fluorescence NCs probes. The analyte, if present, can quench the fluorescence of the NCs, resulting in a decreased fluorescence signal. Shang et al. [135] developed an intracellular Hg^{2+} sensor in HeLa cells by using NIR-emitting dihydrolipoic acid (DHLA)-capped AuNCs. Furthermore, fluorescent AuNCs synthesized using BSA was also applied for the sensing of Cu^{2+} in live cells [136]. In the same way, Wang et al. developed a method for Pb^{2+} detection in aqueous solutions and in living cells via NP aggregation by the synthesis of a pH-responsive copper NC functionalized with GSH [137]. Another smart strategy for intracellular Hg^{2+} imaging was developed by Pu et al. [138] in which a FRET-based hybrid complex nanoprobe using blue-fluorescent conjugated oligomer-substituted polyhedral oligomeric silsesquioxane (POSSFF) and red-fluorescent metal NCs as the energy donor and acceptor, respectively. Because of the specific metallophilic Hg^{2+} interaction on the NC surface, the fluorescence of the complex was significantly quenched by Hg^{2+} rather than other metal ions (Figure 5). Moreover, the whole-cell permeability of the complexes and the preserved ion-selective FRET in cells make these complexes effective for multicolor intracellular sensing of Hg^{2+}. Very recently, Han et al. [139] developed a single fluorescent probe based on the combination of AuNCs, FITC, and 7-diethylaminocoumarin-3-carboxylic acid with ratiometric fluorescence signals. This NC-based nanoprobe showed high selectivity, sensitivity, and accuracy for Cu^{2+}, and was successfully applied in intracellular imaging and sensing of pH and Cu^{2+}, as well as used in ROS regulation of pH and Cu^{2+} changes in macrophage cells.

3. Upconversion nanoparticle-based fluorescent nanoprobes for sensing and imaging of metal ions

Upconversion nanoparticles (UCNPs), a class of rare-earth ion-doped nanoluminophores with excitation wavelengths in the near-infrared (NIR) region [140-146], have been emerging as the ideal nanoprobes for selective sensing and imaging of metal ions both *in*

Author Manuscript Author Manuscript Author Manuscript Author Manuscript

vitro and *in vivo* [147,148], due to their unique properties including tunable multicolor emission, exceptional photostability, deep tissue penetration and suppression of autofluorescence, and low *in vitro* and *in vivo* toxicity [35,149-151]. Therefore much progress has been made in their controlled synthesis, surface engineering, and applications in biomedicine [152-155]. One particular area of interest is their application in metal ion sensing and imaging. Toward this goal, many different design strategies have been developed in which Förster resonance energy transfer (FRET) and luminescence resonance energy transfer (LRET) are two main methods. In the FRET method, a dye or QD is used as an energy acceptor, while an UCNP is used as an energy donor, which offers a larger freedom for upconverted emission wavelengths than the one produced merely by the lanthanide ions. In contrast, the LRET method is a radiative process where light emitted by the donor is absorbed by acceptor molecules [156]. The difference between LRET and FRET methods resides in the energy transfer process which is radiative for LRET but nonradiative for FRET. Stemming from the development of the LRET and FRET methods, various UCNPs based nanoprobes have been designed as sensors for the detection and imaging of metal ions, particularly for heavy metal ions (e.g. Hg^{2+}, Pb^{2+}, Cu^{2+}).

3.1 Detection of metal ions in environmental and biological samples

Metal ions, especially heavy metal ions, have been reported to possess a strong quenching property on the luminescence of UCNPs at certain concentrations (>10 mM). For instance, Saleh et al. [157] have systematically investigated the quenching of UCNPs by heavy metal ions, including Ag^{+}, Cu^{2+}, Hg^{2+}, Pb^{2+}, Cd^{2+}, Co^{2+}, Zn^{2+}, and Fe^{3+}, based on the Stern–Volmer relationship. However, in most cases, the upconversion effect is inert to the target ions. As a result, for sensing and imaging, it is essential to integrate UCNPs with a suitable organic indicator that can recognize the targeted ions. Kumar et al. [156] reported an energy transfer sensor for the detection of Hg^{2+}, in which a DNA modified $NaYF_4$:Yb^{3+}/Tm^{3+} UCNP was employed as an energy donor, while SYBR Green, a DNA intercalating dye, was used as an energy acceptor. In the presence of Hg^{2+}, thymine–Hg^{2+}–thymine was formed and the single stranded DNA folded and trapped the intercalating dye, leading to LRET from the UCNPs to SYBR Green. This method allowed for selective detection of Hg^{2+} with a LOD of 0.06 nM. In another study on developing UCNP-based Hg^{2+} sensors [158], a hydrophobic cyclometallated ruthenium complex was employed as a chemodosimeter to assemble on amphiphilic polymer-coated UCNPs, based on the hydrophobic–hydrophobic interaction (Figure 6). Using the ratiometric upconversion luminescence (UCL) emission at 541 nm to 801 nm as a detection signal, this nanoprobe displayed a LOD of 8.2 ppb for Hg^{2+} with high selectivity. Other Hg^{2+} sensors based on either aptamer [159] or Rhodamine B thiolactone-functionalized UCNPs [160] have also been reported.

Apart from Hg^{2+} detection, various UCNP-based nanoprobes were designed for the selective detection of Pb^{2+} [161-163]. For instance, Xu et al. developed a FRET assay by choosing the upconversion $NaYF_4$:Yb^{3+}/Tm^{3+} NPs as the energy donor and the thioglycolic acid (TGA)-capped CdTe QDs as the energy acceptor for sensitive detection of Pb^{2+} in human serum [161]. The UCNPs and the QDs were assembled together via an electrostatic interaction, which enabled an efficient UC-LRET process from the UCNPs to the QDs. With the

Author Manuscript Author Manuscript Author Manuscript Author Manuscript

addition of Pb^{2+}, TGA capping was preferentially displaced from the surface of the QDs, leading to fluorescence quenching.

Another turn-on nanoprobe for Pb^{2+} was developed by Lv's group [162], where UCNPs capped with positively charged ethylene imine polymer (PEI) and AuNPs capped with negatively charged 11-mercaptoundecanoic acid (MUA) were used as fluorescent donors and acceptors, respectively (Figure 7). The fluorescence of UCNPs was initially quenched by the electrostatic interaction between PEI–UCNPs and MUA–AuNPs (Figure 7A). However, upon addition of Pb^{2+}, the fluorescence of UCNPs was restored due to the departure of AuNPs caused by Pb^{2+}-templated chelation (Figure 7B). The sensor displayed a LOD of 20 nM and good selectivity to other metal ions (Figure 7C). Recently, Wu et al. [164] presented a novel dual FRET system for the simultaneous detection of Pb^{2+} and Hg^{2+} by employing two color UCNPs as the donors, and AuNPs as the acceptors. In the presence of Pb^{2+} and Hg^{2+}, the green and red upconversion fluorescence was restored due to the disruption of the FRET effect, allowing for the quantification of Pb^{2+} and Hg^{2+}, with a LOD of 50 pM and 150 pM, respectively. This assay was also applied for the accurate monitoring of Pb^{2+} and Hg^{2+} levels in samples of naturally contaminated seafood and human serum.

Fluorescent probes based on UCNPs for the detection of Cu^{2+} [165-167], Cr^{3+} [168], Cr^{6+} [169], as well as Na^{+} and Ca^{2+} [170], have also been reported, and have been used in complex biological or environmental samples, including urine, water, and blood.

3.2 Imaging of metal ions within cells and in vivo

Unlike most other optical probes, UCNPs can convert NIR excitation light into shorter-wavelength visible luminescence [171]. This property, combined with their high photostability and low cytotoxicity, make them suitable for intracellular and even deep tissue imaging of metal ions. Liu et al. [172] reported a highly selective nanoprobe for upconversion luminescence sensing of intracellular Hg^{2+}, where a chromophoric ruthenium complex (N719) was assembled on the surface of UCNPs. Hg^{2+} could induce a significant blue shift for the absorption maximum of the complex N719, resulting in a recovery of the upconversion luminescence emission of UCNPs because of decreased spectral overlap. Following this principle, the N719-UCNPs nanoprobe can be used in bioimaging of Hg^{2+} ions in living cells. Later, the same group produced a similar UCNP probe for *in vivo* upconversion luminescence bioimaging of methylmercury ($MeHg^{+}$) [173]. As shown in Figure 8, a hydrophobic heptamethine cyanine dye (hCy7) was modified on the surface of the UCNPs and acted as the $MeHg^{+}$ recognition group. In the presence of $MeHg^{+}$, the hCy7 molecule lost its sulfur atom, followed by a cyclization reaction to give hCy7′, resulting in a significant red shift of the absorbance of the cyanine antennas from 670 to 845 nm, thereby causing a decrease of the UCL at 800 nm. Using the ratiometric upconversion luminescence as a detection signal, which provided a built-in correction for environmental effects, the LOD of $MeHg^{+}$ for this nanosystem was as low as 0.18 ppb. Importantly, the hCy7-UCNPs nanoprobe was shown to be capable of monitoring $MeHg^{+}$ *ex vivo* and *in vivo* by upconversion luminescence bioimaging. Most importantly, the N719-UCNPs nanoprobe was shown to be capable of monitoring changes in the distribution of Hg^{2+} in living cells by upconversion luminescence bioimaging.

Author Manuscript Author Manuscript Author Manuscript Author Manuscript

Very recently, Peng et al. [174] reported the rational design and synthesis of a Zn^{2+} fluorescent-based probe by assembling UCNPs with chromophores (Figure 9). Specifically, upconversion luminescence can be effectively quenched by the chromophores on the surface of nanoparticles via a FRET process and subsequently recovered upon the addition of Zn^{2+}, thus allowing for quantitative monitoring of Zn^{2+}. This chromophore–UCNP nanoprobe has demonstrated the capability for implementing an efficient *in vitro* and *in vivo* detection of Zn^{2+} in mouse brain slices with Alzheimer's disease and in zebrafish.

4. Semiconductor nanoparticle-based fluorescent nanoprobes for sensing and imaging of metal ions

Well-dispersed semiconductor nanocrystals called quantum dots have been revolutionary in the development of fluorescent probes for metal ion sensing [175] and imaging [176-178] due to their unique optical properties including broad absorption, size- and component-tunable emission, as well as high photo- and chemical stability and high quantum yield [179-182] in comparison to traditional organic dyes. The synthesis, surface modification, characterization, and application of QDs in sensing and imaging have been well summarized previously [183]. As a new class of fluorescent probes, QDs show promise in overcoming the limitations of organic dyes and developing new applications for intracellular and in vivo imaging [178,183-185]. In this section, we will focus on their use as a signal reporter for the determination of heavy metal ions both *in vitro* and *in vivo*.

4.1 Undoped quantum dots

Undoped quantum dots (q-dots), including cadmium (Cd) and non-cadmium based QDs, have attracted attention for use in metal ion sensing because of their distinct advantages such as narrow and symmetric emission with tunable colors, broad and strong absorption, low scattering, reasonable stability, and solution processability [175-177]. In QD-based metal ion sensors, interaction between QDs and metal ions are detected as photoluminescence changes caused by either direct physical adsorption or selective binding of metal ions on the QD surface functionalized with metal ion selective receptors. In general, the direct absorption of metal ions by QDs is a very complicated process and several interaction pathways have been summarized elsewhere [176]. On the other hand, functionalization of the QDs with metal ion-selective receptors reduces non-specific interactions. Furthermore, FRET-based sensors using QDs as energy donors were recently developed and applied for sensing of various metal ions [185-188], offering a fast, sensitive, and non-destructive method for metal ion measurement.

4.1.1 Detection of metal ions in environmental and biological samples—

Because of the high emission quantum yields and size-tunable emission profiles, QDs have become one of the most extensively used optical sensing nanomaterials in the detection of metal ions [176]. For instance, Chen et al. [189] utilized thioglycerol-capped CdS QDs as an ion-selective probe to determine copper, zinc, and ferric ions in buffer solutions. Due to the effect on photoluminescence (PL) behaviors of QDs by metals ions, QDs have also been utilized as fluorescent probes for many metal ions, including K^+ [188], Ag^+ [190], Cd^{2+} [191,192], Cu^{2+} [193-200], Fe^{2+}, Hg^{2+} [187,201-207], Pb^{2+} [208], Cr^{3+} [209,210],

Author Manuscript Author Manuscript Author Manuscript Author Manuscript

Fe^{3+} [211], Sb^{3+} [212], Co^{2+} [213], Ba^{2+} [214], Ca^{2+} and Ni^{2+} [215]. Based on this principle of direct interaction of metal ions with QDs, the Zhu group [195] reported L-cysteine-capped NIR-emitting CdSeTe QDs for selective detection of Cu^{2+}, with a LOD of 7.1 nM. The fluorescence quenching of QDs by Cu^{2+} was mainly attributed to the competitive binding of cysteine with Cu^{2+}. The sensor has also been successful for the detection of Cu^{2+} in vegetable samples including bean, cucumber and tomato.

Based on the principles of FRET, Wu et al. [216] developed a DNAzyme-based biosensor for the detection of heavy metal ions in liquid. In order to reach the higher quenching efficiency, dual-quenchers were modified on the substrate and DNAzyme segment. The ZnS-capped CdSe QD was embedded in a siloxane shell and covalently coupled to DNAzymes (Figure 10A). Each DNAzyme was composed of two quenchers and the fluorescence from the QD was quenched by the quenchers in the absence of target metal ions. Once the target metal ion bound to the DNAzyme, the cleavage of the DNAzyme substrate resulted in the separation of the quencher from the QD, which restored the fluorescence from the QD. With two different colors of QDs, this method could also be used in multiplexed detection of Pb^{2+} and Cu^{2+}. The detection limits for Pb^{2+} and Cu^{2+} were 0.2 and 0.5 nM, which was a 50- and 70-fold improvement over those methods based on dye molecules. Similarly, sensing methods using QD-based FRET were also applied in the detection of Hg^{2+} [92], Pb^{2+} [217], Ag^{+} [218], Mg^{2+} [78], and Ca^{2+} [219].

Another smart transducer-based sensing method was recently developed by the Dai group [220], in which analyte ions reacted with a transducer to produce a new chemical intermediate, causing quenching of the QD fluorescence (Figure 10B). Their sensor was composed of CdTe QDs, methanol, and alcohol oxidase (AO). AO catalyzed the oxidation of methanol to produce hydrogen peroxide, resulting in quenching of the QD fluorescence. It is important to note that Cu^{2+} ions could react with AO and inhibit the activity, therefore reducing the quenching of QD fluorescence. Other metal ions showed no significant inhibition to AO activity, and the LOD for Cu^{2+} ions was found to be as low as 2.75 nM. The practical application of this QD–enzyme hybrid system was also demonstrated in domestic waste water, agricultural irrigation water and lake water analysis. Similarly, sensitive photoluminescent detection of Cu^{2+} in a river water sample and Cu^{2+} complexed by amino acids and proteins in cerebrospinal fluids was reported by using CdS QDs in combination with a Cu^{2+}-reducing reaction [221].

4.1.2 Imaging of metal ions within cells and in vivo—The intracellular detection of heavy metal ions has gained significant attention due to its biological implications. Considerable efforts have been made for the sensing of heavy metals such as Hg^{2+} [222], and Zn^{2+} [185,223] using QD nanoprobes based either on fluorescence enhancement or quenching in living cells. One such effort was led by the Zhu group [224] who reported a microwave-assisted synthesis of highly luminescent AgInS/ZnS QDs with good selectivity and sensitivity for Cu^{2+}. In this study, the dynamic changes of the intracellular Cu^{2+} levels in HeLa cells were monitored using the QDs as fluorescent probes. Yet another example is the work of Fu et al. [225]. By developing a ratiometric two-photon fluorescent probe (Figure 11), ATD@QD-E_2Zn_2SOD (ATD = amino triphenylamine dendron, QD = CdSe/ZnSe quantum dot, E_2Zn_2SOD = Cu-free derivative of bovine liver copper–zinc superoxide

Author Manuscript Author Manuscript Author Manuscript Author Manuscript

dismutase). With this system, fluctuations of intracellular Cu^{2+} levels could be imaged through a clear red-to-yellow color change based on specific biomolecular recognition of E_2Zn_2SOD for Cu^{2+}. The hybrid fluorescent probe featured two independent emission peaks located at 515 nm for ATD and 650 nm for QDs, respectively, under two-photon excitation at 800 nm. Upon addition of Cu^{2+} ions, the red fluorescence of QDs was drastically quenched, while the green emission from ATD stayed constant and served as a reference signal, thus resulting in ratiometric detection of Cu^{2+} with high accuracy by two-photon microscopy (TPM). The present probe showed high sensitivity, a broad linear range (10^{-7}–10^{-3} M), low LOD down to ~10 nM, and excellent selectivity over other metal ions, amino acids, and biological species. Meanwhile, this QD-based inorganic-organic probe demonstrated long-term photostability, good cell-permeability, and low cytotoxicity. As a result, the present probe can visualize Cu^{2+} changes in live cells by TPM.

Another FRET ratiometric fluorescence sensing system for the detection and intracellular imaging of Hg^{2+} in live HeLa cells was developed by Hu et al. [222] using N-acetyl-L-cysteine functionalized QDs (NAC-QDs) as the donor and a Rhodamine 6G derivative-mercury conjugate (R6G-D-Hg) as the acceptor. In this system, mercury annihilated the fluorescence of NAC-QDs at 508 nm and also interacted with the R6G derivative to form a fluorescent conjugate, giving rise to emission at 554 nm. Resonance energy transfer from NAC-QDs to R6G-D-Hg was triggered by mercury, resulting in concentration-dependent variation of the fluorescence ratio: F_{508}/F_{554}. In another case, Wu et al. [226] reported the design and synthesis of a new ratiometric fluorescent probe (Figure 12), containing different-colored QDs as dual fluorophores, an ultrathin silica shell as the spacer, and meso-tetra(4-sulfonatophenyl)porphine dihydrochloride as the receptor, which was successfully applied for imaging and biosensing of Zn^{2+} in living cells (Figure 12).

4.2 Doped quantum dots

Despite substantial progress made in using undoped QDs in sensing and imaging, the self-quenching of undoped QDs due to either the intramolecular ground-state dimer complex or to the energy transfer between adjacent QDs may hamper their applications in bioanalysis [227]. To overcome this limitation, much effort has been made to add dopants into pure QDs to enhance their performance [228-236]. Doped QDs can not only potentially retain almost all of the advantages of q-dots, but can also avoid the self-quenching problem due to their substantial ensemble Stokes shift [227]. To date, a variety of transition-metal and lanthanide-metal ions, including Mn^{2+}, Cu^{2+}, Co^{2+}, Ni^{2+}, Ag^{+}, Pb^{2+}, Cr^{3+}, Eu^{3+}, Sm^{3+}, and Er^{3+}, have been doped into QDs, making doped QDs attractive for diverse applications in metal ion sensing and imaging [177,178,227,237].

4.2.1 Detection of metal ions in environmental and biological samples—Unlike undoped QDs, only a few doped QD-based fluorescent sensors were developed on the basis of direct interaction between analytes and non-specifically functionalized doped QDs. Not surprisingly, the selectivity of such approaches is quite limited. To improve the selectivity, the surface of the doped QDs was modified with metal ion-specific ligands [231]. For instance, Huang et al. [232] designed a “turn-on” fluorescent sensor for determination of Hg^{2+} based on the Hg^{2+}-induced conformational change of thymine-rich ssDNA and the

Author Manuscript Author Manuscript Author Manuscript Author Manuscript

water-soluble, long-lifetime Mn:CdS/ZnS QDs. As shown in Figure 13, strand A was attached to Mn:CdS/ZnS QDs, which were linked to AuNPs conjugated with strand B through hybridization of the DNA strands. This resulted in energy transfer from the QDs to the AuNPs, leading to a decrease in the time-gated fluorescence intensity of QDs. In the presence of Hg^{2+}, Hg^{2+}-mediated base pairs induced the folding of strand A into a hairpin structure, leading to release of the AuNP-strand B complexes, and thus the recovery of QD fluorescence. This sensor exhibited a LOD of 0.18 nM for Hg^{2+}. Similarly, based on C-Ag^{+}-C coordination chemistry, a "turn-off" fluorescent sensor for Ag^{+} was developed using Mn:CdS/ZnS QDs/DNA/AuNP complexes [233]. Based on the phosphorescence quenching effect of enlargement caused by hydroxyl radicals, Jin et al. reported a Mn:doped ZnS-QD hybrid for the selective detection of Fe^{2+} [234], through production of hydroxyl radicals by the Fenton reaction. Hg^{2+} ions were also detected using Mn:doped ZnS QDs [235] and ZnSe/ZnS QDs [236].

4.2.2 Imaging of metal ions within cells and in vivo—An increasing amount of attention is being paid to the detection of intracellular Zn^{2+} because of its diverse and important roles in biological systems. In particular, the Yan [237] group developed QD-based photoluminescence imaging for intracellular Zn^{2+} (Figure 14A). Silica-coated S^{2-}-enriched Mn-doped ZnS QDs (SiO_2-S-Mn-ZnS QDs) were fabricated by enriching S^{2-} with a silica shell on the surface of Mn-doped ZnS QDs via a sol-gel process for imaging intracellular Zn^{2+}. The silica-coating on the enriched S^{2-} effectively avoided the leakage of S^{2-}, enhancing the biocompatibility and stability, which made the probe promising for imaging intracellular Zn^{2+} (Figure 14B). Recently, a GSH-capped Mn-doped CdS/ZnS/CdS QD has been designed, synthesized, and utilized as a highly efficient nanoprobe for rapid, selective, and ultrasensitive Cu^{2+} detection [238] (Figure 14C). Cu^{2+}-induced non-radiative recombination blocks the energy transfer pathway from the QDs to the Mn dopant, resulting in quenching of Mn^{2+} emission, with a LOD of Cu^{2+} as low as 0.74 nM. Moreover, the nanoprobe was successfully applied for monitoring Cu^{2+} in living cells (Figure 14D).

5. Carbon Materials-based fluorescent nanoprobes for sensing and imaging of metal ions

Carbon nanomaterials can take several shapes and the best known are: fullerene (C60), carbon nanotubes (CNTs): both single-walled (SWCNT) and multiple-walled (MWCNT), nanodiamonds, carbon nanofibers, graphene (which comprises single molecule layered sheets of graphite), and carbon dots (CDs) [239].

5.1 Carbon dots and graphene QDs

Carbon dots (CDs) are synthesized as either carbogenic dots or carbon nanoparticles (CNPs) [15,239,240]. Compared to semiconductor QDs, these luminescent carbon-based nanomaterials demonstrate non-blinking fluorescence emission, excellent water solubility, and non-toxic response [240]. Because of these properties, CDs are widely used as fluorescent probes for the detection of metal ions [241-243]. For example, Guo et al. [244] developed a simple, one-step hydrothermal method for the synthesis of highly fluorescent CNPs with a high quantum yield (68%) and good photo-stability, and can be used to detect

Author Manuscript Author Manuscript Author Manuscript Author Manuscript

Hg^{2+} in an aqueous solution. CDs have also been used to detect other ions such as Sn^{2+}, Cu^{2+}, Ag^{+}, and Al^{3+} [245].

Recently, Yuan et al. [246] reported a new fluorescence turn-on nanosensor for the selective detection of Hg^{2+} with bis(dithiocarbamato)copper(II) ($CuDTC_2$) functionalized CNPs **(Figure 15A).** They synthesized amine-coated CNPs and conjugated $CuDTC_2$ complexes on their surfaces through condensation between carbon disulfides and nitrogen atoms in the surface amine groups. The conjugated $CuDTC_2$ complex on the surface of CNPs can effectively quench the fluorescence of CNPs due to the combination of electron and energy transfer. The addition of Hg^{2+} can lead to recovery of the fluorescence of CNPs because the conjugated Cu^{2+} is replaced by Hg^{2+}, cutting off the energy transfer pathway (Fig. 15A). The nanosensor can detect Hg^{2+} with a LOD as low as 20 nM. Interestingly, the nanosensor can be fabricated onto paper and acts as a portable Hg^{2+} nanosensor. This fluorescence turn-on nanosensor can eliminate disturbance from the detection medium and could possibly be developed for the detection of other metal ions with CNPs. Ratiometric fluorescent probes have recently attracted interest because of their high accuracy. Cao et al. [247] have constructed a ratiometric fluorescent nanosensor for Hg^{2+} (Figure 15B) through simple mixing of the blue-emission CNPs with red-emission carboxylmethyldithiocarbamate modified CdSe@ZnS QDs (GDTC-QDs). The hybrid nanosensor showed dual emissions at 436 nm and 629 nm at a single excitation wavelength (365 nm). Because of the strong chelating ability of GDTC to Hg^{2+}, the fluorescence of GDTC-QDs in the hybrid nanosensor can be effectively quenched by Hg^{2+}, but the fluorescence of CNPs remained constant, resulting in a continuous fluorescence color change from red to blue with an increase of the concentration of Hg^{2+}. This nanosensor exhibited a LOD of 0.1 μM. This method can effectively eliminate disturbance from the detection medium because the fluorescence of CNPs can be used as the standard signal. More importantly, this strategy can easily be adapted for the detection of other metal ions just by changing the ligands on the surface of QDs. The above mentioned F-CNPs can detect Hg^{2+} in aqueous solution with proper surface modification.

CDs show size dependent photoluminescence and upconversion luminescence properties due to a multi-photon process, which leads to anti Stokes type emission [242]. Due to the biocompatibility of the carbon materials, they can be readily used in biological applications [242]. The Tian group integrated an organic molecule specific for Cu^{2+} ions into a hybrid system composed of carbon and CdSe/ZnS QDs (Figure 16A), allowing for a selective and sensitive ratiometric strategy for intracellular sensing and imaging of Cu^{2+} [248]. The fluorescent probe can monitor Cu^{2+} in a concentration range from 5 - 200 μM in a physiological pH environment. Following uptake, the particles were found to reside in various intracellular compartments (Figure 16B). After exogenous Cu^{2+} source treatment, the fluorescence emission color of the probe turned from green-yellow to red. These initial experiments on live cells demonstrated the great potential for CD-based dual-emission hybrid sensors in the investigation of fundamental biological processes. Later, Castillo et al. [249] developed a fluorescent nanosensor for Cu^{2+} detection based on upconversion fluorescence of CDs using UV and NIR as excitation sources. The CDs were prepared by using a one-step microwave method via pyrolysis of citric acid at low temperature and in the

Author Manuscript Author Manuscript Author Manuscript Author Manuscript

presence of polyethylenimine (PEI). The CDs were highly selective for Cu^{2+} detection. However, at an excitation wavelength of 350 nm, Fe^{3+} ions resulted in a dramatic decrease in fluorescence of CDs, attributed to an inner filter caused by its strong absorption at the mentioned excitation wavelength. However, this interference could be eliminated when the excitation was at 850 nm, because Fe^{3+} did not suffer inner filter at this excitation wavelength, a useful advantage of this upconverting NPs. In addition, these fluorescent nanosensors showed low cytotoxicity and good cell permeability, thus they could be successfully used for sensing and imaging of Cu^{2+} in living cells.

Recently, Graphene QDs (GQDs) and their derivatives, including graphene oxide QDs (GOQDs) and reduced graphene QDs (rGOQDs) have been presented [250], and used as fluorescent probes for biomolecular sensing and cellular bioimaging applications [251,252] due to their unique photoluminescence features. GQDs were used to detect Ag^{+} [253], Hg^{2+} [254], Cu^{2+} [255,256], Cr^{6+} [257], Ni^{2+} [258], and Fe^{3+} [259]. The Lee group [260] reported a green synthesis method for graphitic carbon QDs (GCQDs) as a fluorescent sensing platform for the highly sensitive and selective detection of Fe^{3+} ions. The high sensitivity of GCQDs could be attributed to the formation of complexes between Fe^{3+} ions and the phenolic hydroxyls of GCQDs. The Li group [258] carried out a systematic evaluation of the quenching effect of commonly encountered transition metal ions (Sc^{3+}, Cr^{3+}, Mn^{2+}, Fe^{3+}, Co^{2+}, Ni^{2+}, Cu^{2+}, Zn^{2+}, Ru^{3+}, Ag^{+}, Cd^{2+}, and Hg^{2+}) on the PL of GQDs. With GQDs as both the chelator and fluorophore and EDTA as the competitive chelator, quenching-recovery performance of the above metal ions on the photoluminescence of GQDs can be categorized into non-quenching (Sc^{3+}, Zn^{2+}, Ag^{+}, Cd^{2+}, Hg^{2+}), quenching-recovering (Mn^{2+}, Co^{2+}, Ni^{2+}, Cu^{2+}), and quenching-non-recovering groups (Cr^{3+}, Fe^{3+}, Ru^{3+}).

To further improve the recognition specificity, ssDNA aptamer modified probes were introduced to these systems. Li et al. [261] developed the water-soluble GO sheets, which were functionalized with a ssDNA aptamer and, in the absence of Hg^{2+} ions, exhibited a strong fluorescence emission at 600 nm under an excitation of 488 nm. When Hg^{2+} ions were present, a rigid hairpin-shaped dsDNA structure was formed due to the coordination of T-Hg^{2+}-T, Because the Hg^{2+} ions were very close to the surface of the GO sheet, electrons can transfer from GO to the Hg^{2+} ions along the duplex DNA channel, resulting in quenching of the fluorescence emission of GO. Thus, the detection mechanism was based on “turn-off” of the fluorescence of GO. Liu et al. [262] reported a photoluminescent GO array on which heavy metal ion-specific DNA aptamers were immobilized so that sensitive and multiplex heavy metal ion detection was performed utilizing electron transfer between the photoluminescent monolayer GO and the captured metal ion.

The Qu group [263] reported amino-functionalized GQDs (afGQDs) with a high QY (16.4%), which was generated by hydrothermal treatment of greenish-yellow fluorescent GQDs (gGQDs). Due to the fact that Cu^{2+} ions have a higher binding affinity and faster chelating kinetics with N and O on the surface of afGQDs than with other transition metal ions, the selectivity of afGQDs for Cu^{2+} is much higher than that of gGQDs (Figure 17A). Furthermore, amination converted the surface charge of the GQDs from negative to positive,

Author Manuscript Author Manuscript Author Manuscript Author Manuscript

which made it easy for the GQDs to be taken up by cells. Using afGQDs as a fluorescence probe, the profiling of Cu^{2+} in living cells was successfully realized (Figure 17b).

5.2 Carbon nanotubes and graphene oxide

While some carbon-based materials are inherently fluorescent, other carbon materials, such as fullerene, carbon nanotubes and graphene, are powerful fluorescence quenchers [264,265]. Zhang et al. [266] presented a sensitive and selective fluorescent sensor for Hg^{2+} detection that works based on the noncovalent assembly of single-walled carbon nanotubes (SWNTs) and dye-labeled T-rich ssDNA containing thymine–thymine (T–T) mismatches that shows high selectivity for Hg^{2+} against other metal ions, owing to the formation of T–Hg^{2+}–T base pairs (Figure 18A). Similarly, the Sun group [267] reported water-soluble nano-C60 to be an effective fluorescent sensing platform for the detection of Ag^{+} because of the substantial dye fluorescence quenching that occurs when the fluorescently labeled ssDNA probe adsorbs on nano-C60 (Figure 18B). In contrast, in the presence of Ag^{+}, cytosine-Ag^{+}-cytosine (C–Ag^{+}–C) coordination induced the probe to fold into a hairpin structure, which did not adsorb on nano-C60 and thus retained the dye fluorescence. This sensing system exhibited a LOD as low as 1 nM and had a high selectivity against other metal ions. The Qu group [268] have developed a reusable DNA SWNT-based fluorescent sensor for highly sensitive and selective detection of Ag^{+} and cysteine (Cys) in aqueous solution. SWNTs can effectively quench the fluorescence of dye-labeled single-stranded DNA due to their strong **π**–**π** stacking interactions. However, upon incubation with Ag^{+}, stable duplex formation can be induced, mediated by C–Ag^{+}–C coordination chemistry, which has been further confirmed by DNA melting point studies. This weakens the interactions between DNA and SWNTs, activating the sensor fluorescence. On the other hand, because Cys is a strong Ag^{+} binder, it can remove Ag^{+} from C–Ag^{+}–C base pairs and deactivates the sensor fluorescence by rewrapping the dye-labeled oligonucleotides around the SWNT.

In addition to the low concentrations of heavy metal ions, detection of these metal ions in real samples is often complicated by the presence of other metal ions, making their determination a difficult task. To overcome this limitation, Wang et al. [264] developed a novel aptamer biosensor based on MWCNT long-range energy transfer for sensitive, selective and multicolor fluorescent detection of Hg^{2+}, Ag^{+} and Pb^{2+} ions in homogeneous solution. Three-color nanosensors can rapidly and simultaneously detect these three metal ions in a single solution. This MWCNT-based sensing platform exhibited high sensitivity and selectivity toward Hg^{2+}, Ag^{+} and Pb^{2+} versus other metal ions, with a LOD of 15 nM for Hg^{2+}, 18 nM for Ag^{+} and 20 nM for Pb^{2+}.

Since its discovery, graphene has been widely used in bioassays [269-271]. GO is an extraordinary optical sensing material that can serve either as an energy acceptor or as an energy donor for a fluorophore. Functional DNAs [272-275], such as aptamers [276], have been used as metal-ion specific receptors for sensitive and selective metal ion detection [277,278]. For instance, the Ye group [279] has developed a ssDNA–GO architecture probe for multiplex detection of sequence-specific DNA, thrombin, Ag^{+}, Hg^{2+} and cysteine, with a LOD of 1 nM, 5 nM, 20 nM, 5.7 nM and 60 nM, respectively (Figure 18C). Another

Author Manuscript Author Manuscript Author Manuscript Author Manuscript

example came from the Fan group [280] who developed a mix-and-detect fluorescent sensor for Ag^+ by using a silver-specific oligonucleotide (SSO) probe that can be coupled with the ability of GO to specifically adsorb and quench single stranded fluorogenic DNA probes. For this sensor, a FAM labeled SSO containing cytosine (C)-rich nucleic acids separated by a spacer was used as a fluorescence probe for Ag^+. In the absence of Ag+, the SSO was in a flexible single strand state. Upon addition of Ag^+, the complexation of Ag^+ with the cytosine bases of SSO yielded a rigid hairpin structure. Then, GO was added to selectively adsorb the unbound SSO and quench its fluorescence, while the Ag^+ complexed with SSO remained free and its fluorescence was retained. Through this method, the fluorescence intensity of SSO provided a quantitative readout for Ag^+. In yet another example, Zhang et al. [281] reported a graphene oxide (GO)-based fluorescence Hg^{2+} analysis using DNA duplexes of poly(dT) that allows rapid, sensitive, and selective detection via stable T–Hg^{2+}–T complexes. Finally, Li et al. [282] developed a rapid, sensitive and selective fluorescent sensor for detection of Pb^{2+} based on a Pb^{2+}-induced G-quadruplex on GO.

In addition to aptamers described above, DNAzymes have been investigated due to their high metal ion specificity [283-289]. Various optical sensors for metal ions were developed using graphene and DNAzymes [290-294]. For instance, the Yu group [292] constructed a graphene DNAzyme-based sensing system for amplified fluorescence “turn-on” detection of Pb^{2+}. The 5′ end of the substrate strand is labeled with the fluorophore carboxyfluorescein (FAM), which was hybridized with the DNAzyme strand to form a DNAzyme-substrate hybrid containing a large ssDNA loop (containing 15 bases) which can bind to the surface of the GO and thus induce quenching of the labeled FAM fluorophore. Upon addition of Pb^{2+}, the DNAzyme was activated which induces cleavage of the substrate strand at the single RNA site into two separate strands. This releases a short FAM-linked oligonucleotide fragment, a related longer oligonucleotide fragment, and the DNAzyme strand. The DNAzyme strand can hybridize with another substrate strand and thus induce a second cycle of cleavage upon binding of Pb^{2+}, providing an amplified detection signal for Pb^{2+} (LOD of 300 pM). A novel label free fluorescent Cu^{2+} sensor based on internal DNA cleavage and an extrinsic fluorophore in a graphene/DNAzymes complex was also designed [295], with a LOD of 2 nM.

Combining the fluorescent properties with fluorescence quenching ability of carbon materials, Wei et al. [296] designed a FRET sensor which could be used for measuring the concentration of K^+ with high selectivity (e.g. 37-fold against Na^+) and tunable dynamic range (0-200 mM) via energy transfer from CDs (the donor) to graphene (the acceptor) (Figure 18D). For this sensor to function, energy transfer was induced when CDs and graphene were brought into appropriate proximity by covalently aminated CDs and noncovalently functionalized graphene with 18-crown-6 ether (18C6E). The FRET process was inhibited because of competition between K^+ and ammonium for 18C6E, which had high K^+ selectivity.

6. Conclusion and Future Directions

In summary, we have provided a review of exciting recent advancements of fluorescent nanoprobes in the areas of sensitive and selective sensing and imaging of metal ions, both in

Author Manuscript Author Manuscript Author Manuscript Author Manuscript

vitro and in vivo since 2010. These results reveal that fluorescent nanoprobes can provide excellent tools for investigations in biochemical and biomedical science and engineering. To realize its full potentials, more efforts should be devoted to improving nanoprobe sensitivity and selectivity, expanding the family of detectable metal ions, developing new sensing mechanisms, shifting the nanoprobe excitation and emission spectra towards the NIR region, and functionalization of nanoprobes with multiple modalities. Moreover, in order to design fluorescent nanoprobes that are capable of entering a cell and remaining active in the cellular environment, more investigation should be conducted to improve their biological membrane penetration, as well as for their intracellular stability. More attention should also be paid on the potential toxicity resulting from accumulation of nanoprobes in the lungs through inhalation or by penetration through the skin due to their small size and increased surface area-to-volume ratio, both of which may be minimized by surface modification of nanoprobes to improve their biocompatibility.

Another exciting area of future development is the multiplexed detection of different metal ions simultaneously. Although a few studies using multi-color QDs and dyes have shown promise, the number of metal ion species that can be analyzed in one test is still limited. Not only are new fluorescent nanoprobes needed for other metal ions, but selective receptors compatible for the detection of many metal ions are also required. To satisfy these needs, new multifunctional nanoprobes can be developed through direct integration of different types of building units, and metal ion specific receptors can be identified through either new discoveries in biochemical systems or through new combinatorial selections in test tubes. Given the exciting progresses made so far, we believe that more and better fluorescent nanoprobes will be developed by many researchers, resulting in further significant breakthroughs in biomedical imaging of living systems.

Acknowledgements

We wish to thank Ms. Aileen Nolan and Mr. Ryan Lake for proof-reading, Lu and Zhu group members who contributed to the work described in this chapter, and the U.S. National Institutes of Health (ES16865), Department of Energy (DE-FG02-08ER64568), and US National Science Foundation (CTS-0120978) for financial support. JJZ thanks the support from National Science Foundation of China (No. 21335004).

Author’s Biographical Sketch

JingJing Zhang received his PhD degree in chemistry under the supervision of Prof. Jun-Jie Zhu from the School of Chemistry and Chemical Engineering, Nanjing University, in 2010. Currently he worked as a postdoctoral research associate in the group of Prof. Yi Lu at University of Illinois Urbana-Champaign, since March 2012. His research interests focus on

Author Manuscript Author Manuscript Author Manuscript Author Manuscript

interfacing carbon and gold nanomaterials with biological systems, to develop novel tools for imaging, sensing and diagnostics.

Fangfang Cheng received her BS degree from Yangzhou University in 2008 and PhD degree from Nanjing University in 2014 under the supervision of Prof. Jun-Jie Zhu. Now she is an instructor at the Nanjing University of Chinese medicine. Her research focuses on the synthesis of fluorescence probes and their bioimaging application in the toxicity mechanism of Chinese medicine.

Jingjing Li obtained her BSc in Chemistry Education in 2005 and MSc in Analytical Chemistry in 2008 from Soochow University. Then she received her PhD in 2012 from Nanjing University under the supervision of Prof. Jun-Jie Zhu and Jian-Rong Zhang. During her PhD study she stayed in the group of Prof. X. Chris Le in the University of Alberta as a joint PhD student for 18 months. Currently, she is an associate professor at Xuzhou Medical College. Her primary research interests include the synthesis of novel functionalized nanomaterials and exploration of their applications in the biological area.

Jun-Jie Zhu is a Professor of Chemistry at Nanjing University, China. He received his BS (1984), and PhD (1993) degrees in Chemistry from Nanjing University. After this, he started his academic career at Nanjing University in 1993. During 1998–1999, he was a postdoctoral fellow in Bar-Ilan University, Israel. His current research interests are analytical chemistry and materials chemistry, which mainly focus on the study of nanobioanalytical

Author Manuscript Author Manuscript Author Manuscript Author Manuscript

chemistry including bioelectrochemistry, nanoelectrochemistry and the fabrication of biosensors. The synthesis of functional nanoparticles was also performed.

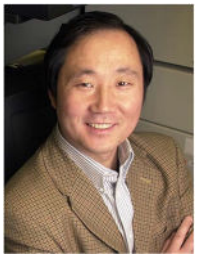

Yi Lu received his BS degree from Peking University in 1986, and a PhD degree from University of California at Los Angeles in 1992 under Professor Joan S. Valentine. After 2 years of postdoctoral research in Professor Harry B. Gray's group at the California Institute of Technology, Lu started his own independent career in the Department of Chemistry at the University of Illinois at Urbana Champaign in 1994. He is now a Jay and Ann Schenck Professor of Chemistry in the Departments of Chemistry, Biochemistry, Bioengineering and Materials Science and Engineering. He is also a member of the Center for Biophysics and Computational Biology and Beckman Institute for Advanced Science and Technology. His research interests include a) design and engineering of functional metalloproteins as environmentally benign catalysis in renewable energy generation and pharmaceuticals; b) Fundamental understanding of DNAzymes and their applications in environmental monitoring, medical diagnostics, and targeted drug delivery; and c) Employing principles from biology for directed assembly of nanomaterials with controlled morphologies and its applications in imaging and medicine.

References

[1]. Dean KM, Qin Y, Palmer AE. Biochim. Biophys. Acta. 2012; 1823:1406–1415. [PubMed: 22521452]

[2]. Qian X, Xu Z. Chem. Soc. Rev. 2015; 44:4487–4493. [PubMed: 25556818]

[3]. Carter KP, Young AM, Palmer AE. Chem. Rev. 2014; 114:4564–4601. [PubMed: 24588137]

[4]. Zhu G, Zhang C.-y. Analyst. 2014; 139:6326–6342. [PubMed: 25356810]

[5]. Sareen D, Kaur P, Singh K. Coord. Chem. Rev. 2014; 265:125–154.

[6]. Zhang XB, Kong RM, Lu Y. Annu. Rev. Anal. Chem. 2011; 4:105–128.

[7]. Yi L. Proc. Natl. Acad. Sci. U.S.A. 2010; 107:1811–1812. [PubMed: 20133828]

[8]. Chen YC, Bai Y, Han Z, He WJ, Guo ZJ. Chem. Soc. Rev. 2015; 44:4517–4546. [PubMed: 25747236]

[9]. Yang Q, Wang L, Zhou Q, Huang X. Ecotoxicol. Environ. Saf. 2015; 111:48–58. [PubMed: 25450914]

[10]. Špirić Z, Vučković I, Stafilov T, Kušan V, Frontasyeva M. Arch. Environ. Contam. Toxicol. 2013; 65:33–46. [PubMed: 23467710]

[11]. Drennan-Harris LR, Wongwilawan S, Tyson JF. J. Anal. At. Spectrom. 2013; 28:259–265.

[12]. Lee S, Bong S, Ha J, Kwak M, Park S-K, Piao Y. Sensor Aatuat. B-Chem. 2015; 215:62–69.

[13]. Liang Y, Deng B, Shen C, Qin X, Liang S. J. Anal. At. Spectrom. 2015; 30:903–908.

[14]. Lee SJ, Lee JE, Seo J, Jeong IY, Lee SS, Jung JH. Adv. Funct. Mater. 2007; 17:3441–3446.

[15]. Guo Y, Zhang L, Zhang S, Yang Y, Chen X, Zhang M. Biosens. Bioelectron. 2015; 63:61–71. [PubMed: 25058940]

Author Manuscript Author Manuscript Author Manuscript Author Manuscript

[16]. Zhang L, Wang E. Nano Today. 2014; 9:132–157.
[17]. Li J, Zhu J-J, Xu K. Trends Anal. Chem. 2014; 58:90–98.
[18]. Zhang JF, Zhou Y, Yoon J, Kim JS. Chem. Soc. Rev. 2011; 40:3416–3429. [PubMed: 21491036]
[19]. Domaille DW, Que EL, Chang CJ. Nat. Chem. Biol. 2008; 4:168–175. [PubMed: 18277978]
[20]. Lan T, Lu Y. Metal Ions Life Sci. 2012; 10:217–248.
[21]. He Y, Lu Y. Chem. Eur. J. 2011; 17:13732–13742. [PubMed: 22052817]
[22]. Torabi SF, Wu PW, McGhee CE, Chen L, Hwang K, Zheng N, Cheng JJ, Lu Y. Proc. Natl. Acad. Sci. U.S.A. 2015; 112:5903–5908. [PubMed: 25918425]
[23]. Hwang K, Wu PW, Kim T, Lei L, Tian SL, Wang YX, Lu Y. Angew. Chem. Int. Ed. Engl. 2014; 53:13798–13802. [PubMed: 25314680]
[24]. Cepeda-Plaza M, Null EL, Lu Y. Nucleic. Acids Res. 2013; 41:9361–9370. [PubMed: 23939617]
[25]. Zhang XB, Wang ZD, Xing H, Xiang Y, Lu Y. Anal. Chem. 2010; 82:5005–5011. [PubMed: 20481627]
[26]. Lan T, Furuya K, Lu Y. Chem. Commun. 2010; 46:3896–3898.
[27]. Xiang Y, Wang ZD, Xing H, Wong NY, Lu Y. Anal. Chem. 2010; 82:4122–4129. [PubMed: 20465295]
[28]. Shao Q, Xing BG. Chem. Soc. Rev. 2010; 39:2835–2846. [PubMed: 20480074]
[29]. Tan LH, Yue Y, Satyavolu NSR, Ali AS, Wang ZD, Wu YQ, Lu Y. J. Am. Chem. Soc. 2015; 137:14456–14464. [PubMed: 26492515]
[30]. Song TJ, Tang LH, Tan LH, Wang XJ, Satyavolu NSR, Xing H, Wang ZD, Li JH, Liang HJ, Lu Y. Angew. Chem. Int. Ed. Engl. 2015; 54:8114–8118. [PubMed: 26096755]
[31]. Wu JJX, Tan LH, Hwang K, Xing H, Wu PW, Li W, et al. J. Am. Chem. Soc. 2014; 136:15195–15202. [PubMed: 25243485]
[32]. Tan LH, Xing H, Lu Y. Acc. Chem. Res. 2014; 47:1881–1890. [PubMed: 24871359]
[33]. Lohse SE, Murphy CJ. J. Am. Chem. Soc. 2012; 134:15607–15620. [PubMed: 22934680]
[34]. Li J, Cheng F, Huang H, Li L, Zhu J-J. Chem. Soc. Rev. 2015; 44:7855–7880. [PubMed: 26214317]
[35]. Min YZ, Li JM, Liu F, Yeow EKL, Xing BG. Angew. Chem. Int. Ed. Engl. 2014; 53:1012–1016. [PubMed: 24311528]
[36]. Yang YM, Shao Q, Deng RR, Wang C, Teng X, Cheng K, et al. Angew. Chem. Int. Ed. Engl. 2012; 51:3125–3129. [PubMed: 22241651]
[37]. Xu JJ, Zhao WW, Song SP, Fan CH, Chen HY. Chem. Soc. Rev. 2014; 43:1601–1611. [PubMed: 24342982]
[38]. Peng F, Su YY, Zhong YL, Fan CH, Lee ST, He Y. Acc. Chem. Res. 2014; 47:612–623. [PubMed: 24397270]
[39]. Xu H, Li Q, Wang LH, He Y, Shi JY, Tang B, Fan CH. Chem. Soc. Rev. 2014; 43:2650–2661. [PubMed: 24394966]
[40]. Xiang Y, Lu Y. Inorg. Chem. 2014; 53:1925–1942. [PubMed: 24359450]
[41]. Torabi SF, Lu Y. Curr. Opin. Biotech. 2014; 28:88–95. [PubMed: 24468446]
[42]. Xiang Y, Wu PW, Tan LH, Lu Y. Adv. Biochem. Eng. Biot. 2014; 140:93–120.
[43]. Wang F, Liu XG. Chem. Soc. Rev. 2009; 38:976–989. [PubMed: 19421576]
[44]. Wang F, Banerjee D, Liu YS, Chen XY, Liu XG. Analyst. 2010; 135:1839–1854. [PubMed: 20485777]
[45]. Liu XG, Yan CH, Capobianco JA. Chem. Soc. Rev. 2015; 44:1299–1301. [PubMed: 25716767]
[46]. Han SY, Deng RR, Xie XJ, Liu XG. Angew. Chem. Int. Ed. Engl. 2014; 53:11702–11715. [PubMed: 25204638]
[47]. Min YZ, Li JM, Liu F, Padmanabhan P, Yeow EKL, Xing BG. Nanomaterials. 2014; 4:129–154.
[48]. Li JM, Liu F, Shao Q, Min YZ, Costa M, Yeow EKL, et al. Adv. Healthc. Mater. 2014; 3:1230–1239. [PubMed: 24550203]
[49]. Lou Y, Zhao Y, Zhu J-J. Nanoscale Horizons. 2016 DOI: 10.1039/C5NH00039D.
[50]. Willner I, Willner B. Nano. Lett. 2010; 10:3805–3815. [PubMed: 20843088]

Author Manuscript Author Manuscript Author Manuscript Author Manuscript

[51]. Xu H, Li Q, Wang L, He Y, Shi J, Tang B, Fan C. Chem. Soc. Rev. 2014; 43:2650–2661. [PubMed: 24394966]
[52]. Chen M, He X, Wang K, He D, Yang X, Shi H. Trends Anal. Chem. 2014; 58:120–129.
[53]. Wolfbeis OS. Chem. Soc. Rev. 2015; 44:4743–4768. [PubMed: 25620543]
[54]. Peng C, Hu WB, Zhou YT, Fan CH, Huang Q. Small. 2010; 6:1686–1692. [PubMed: 20602429]
[55]. Ruedas-Rama MJ, Walters JD, Orte A, Hall EA. Anal. Chim. Acta. 2012; 751:1–23. [PubMed: 23084048]
[56]. Li Q, Liu L, Liu J-W, Jiang J-H, Yu R-Q, Chu X. Trends Anal. Chem. 2014; 58:130–144.
[57]. Zhou M, Xiao X, Kadi AA, Fun HK, Li J, Zhang Y. Curr. drug targets. 2015; 16:549–559. [PubMed: 25330033]
[58]. Lee H, Kim YP. BMB Rep. 2015; 48:313–318. [PubMed: 25817215]
[59]. Payne CK. Biophys. J. 2013; 104:1394. [PubMed: 23561512]
[60]. Merian J, Gravier J, Navarro F, Texier I. Molecules. 2012; 17:5564–5591. [PubMed: 22576228]
[61]. Zhang J, Fu Y, Xu X, Lakowicz JR. J. Biomed. Opt. 2011; 16:116004(1)–116004(6). [PubMed: 22112109]
[62]. Sandanaraj BS, Gremlich HU, Kneuer R, Dawson J, Wacha S. Bioconjug. Chem. 2010; 21:93–101. [PubMed: 19958018]
[63]. Gong J, Li G, Tang Z. Nano Today. 2012; 7:564–585.
[64]. Wu B, Kuang Y, Zhang X, Chen J. Nano Today. 2011; 6:75–90.
[65]. Guo S, Wang E. Nano Today. 2011; 6:240–264.
[66]. Lu F, Doane TL, Zhu J-J, Burda C. Inorg. Chim. Acta. 2012; 393:142–153.
[67]. Knecht MR, Sethi M. Anal. Bioanal. Chem. 2009; 394:33–46. [PubMed: 19189085]
[68]. Zhang JJ, Gu MM, Zheng TT, Zhu JJ. Anal. Chem. 2009; 81:6641–6648. [PubMed: 20337377]
[69]. Zhang JJ, Liu YG, Jiang LP, Zhu JJ. Electrochem. commun. 2008; 10:355–358.
[70]. Zhang JJ, Cheng FF, Zheng TT, Zhu JJ. Anal. Chem. 2010; 82:3547–3555. [PubMed: 20369831]
[71]. Oliveira E, Genovese D, Juris R, Zaccheroni N, Capelo JL, Raposo MM, et al. Inorg. chem. 2011; 50:8834–8849. [PubMed: 21848259]
[72]. Lai JP, Niu WX, Luque R, Xu GB. Nano Today. 2015; 10:240–267.
[73]. Zhang L, Niu WX, Xu GB. Nano Today. 2012; 7:586–605.
[74]. Guo SJ, Wang EK. Nano Today. 2011; 6:240–264.
[75]. Son H, Lee JH, Kim YR, Lee IS, Han S, Liu X, Jaworski J, Jung JH. Analyst. 2012; 137:3914–3916. [PubMed: 22805878]
[76]. Wang S, Sun J, Gao F. Analyst. 2015; 140:4001–4006. [PubMed: 25919909]
[77]. Velu R, Jung S, Won N, Im K, Kim S, Park N. Chemphyschem. 2012; 13:3445–3448. [PubMed: 22887360]
[78]. Velu R, Won N, Kwag J, Jung S, Hur J, Kim S, Park N. New J. Chem. 2012; 36:1725–1728.
[79]. Velu R, Ramakrishnan VT, Ramamurthy P. Tetrahedron Lett. 2010; 51:4331–4335.
[80]. Kaewtong C, Niamsa N, Wanno B, Morakot N, Putpoka B, Tuntulani T. New J. Chem. 2014; 38:3831–3839.
[81]. Tira DS, Focsan M, Ulinici S, Maniu D, Astilean S. Spectrosc. Lett. 2014; 47:153–159.
[82]. Hormozi-Nezhad MR, Taghipour M. Anal. Methods. 2015; 7:5067–5073.
[83]. Wu YS, Huang FF, Lin YW. ACS Appl. Mater. Interfaces. 2013; 5:1503–1509. [PubMed: 23369297]
[84]. Liu J. Trends Anal. Chem. 2014; 58:99–111.
[85]. Wang H-B, Wang L, Huang K-J, Xu S-P, Wang H-Q, Wang L-L, et al. New J. Chem. 2013; 37:2557–2563.
[86]. Wang L, Jin Y, Deng J, Chen G. Analyst. 2011; 136:5169–5174. [PubMed: 22029044]
[87]. He YL, Tian JN, Zhang JN, Chen S, Jiang YX, Hu K, Zhao YC, Zhao SL. Biosens. Bioelectron. 2014; 55:285–288. [PubMed: 24389392]
[88]. Xie WY, Huang WT, Zhang JR, Luo HQ, Li NB. J. Mater. Chem. 2012; 22:11479.

Author Manuscript Author Manuscript Author Manuscript Author Manuscript

[89]. Chhatwal M, Kumar A, Singh V, Gupta RD, Awasthi SK. Coord. Chem. Rev. 2015; 292:30–55.
[90]. Kim YS, Jurng J. Analyst. 2011; 136:3720–3724. [PubMed: 21799952]
[91]. Yin BC, Zuo P, Huo H, Zhong XH, Ye BC. Anal. biochem. 2010; 401:47–52. [PubMed: 20159005]
[92]. Li M, Wang Q, Shi X, Hornak LA, Wu N. Anal. Chem. 2011; 83:7061–7065. [PubMed: 21842845]
[93]. di Gennaro AK, Gurevich L, Skovsen E, Overgaard MT, Fojan P. Phys. Chem. Chem. Phys. 2013; 15:8838–8844. [PubMed: 23646357]
[94]. Tseng CW, Chang HY, Chang JY, Huang CC. Nanoscale. 2012; 4:6823–6830. [PubMed: 23011048]
[95]. Wu P, Hwang K, Lan T, Lu Y. J. Am. Chem. Soc. 2013; 135:5254–5257. [PubMed: 23531046]
[96]. Liu D, Wang S, Swierczewska M, Huang X, Bhirde AA, Sun J, Wang Z, Yang M, Jiang X, Chen X. ACS nano. 2012; 6:10999–11008. [PubMed: 23121626]
[97]. Lee HY, Son H, Lim JM, Oh J, Kang D, Han WS, Jung JH. Analyst. 2010; 135:2022–2027. [PubMed: 20574565]
[98]. Yusop RM, Unciti-Broceta A, Johansson EMV, Sánchez-Martín RM, Bradley M. Nat. Chem. 2011; 3:239–243. [PubMed: 21336331]
[99]. Chen LY, Wang CW, Yuan Z, Chang HT. Anal. Chem. 2015; 87:216–229. [PubMed: 25275676]
[100]. Cui M, Zhao Y, Song Q. Trends Anal. Chem. 2014; 57:73–82.
[101]. Yuan X, Luo Z, Yu Y, Yao Q, Xie J. Chem. Asian J. 2013; 8:858–871. [PubMed: 23512702]
[102]. Yu P, Wen X, Toh Y-R, Ma X, Tang J. Part. Part. Syst. Char. 2015; 32:142–163.
[103]. Zhao T, Zhou T, Yao Q, Hao C, Chen X. J. Environ. Sci. Health., Part C. 2015; 33:168–187.
[104]. Shang L, Dong S, Nienhaus GU. Nano Today. 2011; 6:401–418.
[105]. Zhou C, Yang S, Liu J, Yu M, Zheng J. Exp. Biol. Med. 2013; 238:1199–1209.
[106]. Yuan Z, Chen YC, Li HW, Chang HT. Chem. Commun. 2014; 50:9800–9815.
[107]. Hu Y, Guo W, Wei H. Isr. J. Chem. 2015; 55:682–697.
[108]. Senthamizhan A, Celebioglu A, Uyar T. Sci. Rep. 2015; 5:10403. [PubMed: 26020609]
[109]. Kawasaki H, Hamaguchi K, Osaka I, Arakawa R. Adv. Func. Mater. 2011; 21:3508–3515.
[110]. Gui R, Jin H. Analyst. 2013; 138:7197–7205. [PubMed: 24106735]
[111]. Liu H, Zhang X, Wu X, Jiang L, Burda C, Zhu JJ. Chem. Commun. 2011; 47:4237–4239.
[112]. Vilar-Vidal N, Rivas J, Lopez-Quintela MA. Phys. Chem. Chem. Phys. 2014; 16:26427–26430. [PubMed: 25121465]
[113]. Goswami N, Giri A, Bootharaju MS, Xavier PL, Pradeep T, Pal SK. Anal. Chem. 2011; 83:9676–9680. [PubMed: 22050123]
[114]. Xie J, Zheng Y, Ying JY. Chem. Commun. 2010; 46:961–963.
[115]. Wei H, Wang Z, Yang L, Tian S, Hou C, Lu Y. Analyst. 2010; 135:1406–1410. [PubMed: 20411205]
[116]. Wang C, Xu L, Wang Y, Zhang D, Shi X, Dong F, Yu K, Lin Q, Yang B. Chem. Asian j. 2012; 7:1652–1656. [PubMed: 22499534]
[117]. Guha S, Roy S, Banerjee A. Langmuir. 2011; 27:13198–13205. [PubMed: 21913719]
[118]. Lin YH, Tseng WL. Anal. Chem. 2010; 82:9194–9200. [PubMed: 20954728]
[119]. Zhou T, Huang Y, Li W, Cai Z, Luo F, Yang CJ, Chen X. Nanoscale. 2012; 4:5312–5315. [PubMed: 22837049]
[120]. Chang H-Y, Chang H-T, Hung Y-L, Hsiung T-M, Lin Y-W, Huang C-C. RSC Adv. 2013; 3:4588–4597.
[121]. Hu D, Sheng Z, Gong P, Zhang P, Cai L. Analyst. 2010; 135:1411–1416. [PubMed: 20419194]
[122]. Deng L, Ouyang X, Jin J, Ma C, Jiang Y, Zheng J, Li J, Li Y, Tan W, Yang R. Anal. Chem. 2013; 85:8594–8600. [PubMed: 23937672]
[123]. Deng L, Zhou Z, Li J, Li T, Dong S. Chem. Commun. 2011; 47:11065–11067.
[124]. Liu J, Ren X, Meng X, Fang Z, Tang F. Nanoscale. 2013; 5:10022–10028. [PubMed: 24056730]

Author Manuscript Author Manuscript Author Manuscript Author Manuscript

[125]. Kim HN, Ren WX, Kim JS, Yoon J. Chem. Soc. Rev. 2012; 41:3210–3244. [PubMed: 22184584]
[126]. Yuan Z, Peng M, He Y, Yeung ES. Chem. Commun. 2011; 47:11981–11983.
[127]. Ji L, Guo Y, Hong S, Wang Z, Wang K, Chen X, et al. RSC Adv. 2015; 5:36582–36586.
[128]. Ganguly M, Mondal C, Jana J, Pal A, Pal T. Langmuir. 2014; 30:348–357. [PubMed: 24359547]
[129]. Wu Z, Wang M, Yang J, Zheng X, Cai W, Meng G, Qian H, Wang H, Jin R. Small. 2012; 8:2028–2035. [PubMed: 22488747]
[130]. Yue Y, Liu TY, Li HW, Liu Z, Wu Y. Nanoscale. 2012; 4:2251–2254. [PubMed: 22382936]
[131]. Ngamdee K, Tuntulani T, Ngeontae W. Sensors Actuat. B-Chem. 2015; 216:150–158.
[132]. Ho JA, Chang HC, Su WT. Anal. Chem. 2012; 84:3246–3253. [PubMed: 22364482]
[133]. Zhou TY, Lin LP, Rong MC, Jiang YQ, Chen X. Anal. Chem. 2013; 85:9839–9844. [PubMed: 24016136]
[134]. Sun J, Zhang J, Jin Y. J. Mater. Chem. C. 2013; 1:138–143.
[135]. Shang L, Yang L, Stockmar F, Popescu R, Trouillet V, Bruns M, et al. Nanoscale. 2012; 4:4155–4160. [PubMed: 22460520]
[136]. Durgadas CV, Sharma CP, Sreenivasan K. Analyst. 2011; 136:933–940. [PubMed: 21152627]
[137]. Wang C, Cheng H, Huang Y, Xu Z, Lin H, Zhang C. Analyst. 2015; 140:5634–5639. [PubMed: 26133700]
[138]. Pu K-Y, Luo Z, Li K, Xie J, Liu B. J. Phys. Chem. C. 2011; 115:13069–13075.
[139]. Han Y, Ding C, Zhou J, Tian Y. Anal. Chem. 2015; 87:5333–5339. [PubMed: 25898074]
[140]. Li LL, Zhang R, Yin L, Zheng K, Qin W, Selvin PR, et al. Angew Chem Int Ed Engl. 2012; 51:6121–6125. [PubMed: 22566291]
[141]. Li LL, Wu PW, Hwang K, Lu Y. J. Am. Chem. Soc. 2013; 135:2411–2414. [PubMed: 23356394]
[142]. Li LL, Lu Y. J. Am. Chem. Soc. 2015; 137:5272–5275. [PubMed: 25853565]
[143]. Ding YJ, Zhu H, Zhang XX, Gao JG, Abdel-Halim ES, Jiang LP, et al. Nanoscale. 2014; 6:14792–14798. [PubMed: 25359598]
[144]. Wang F, Han Y, Lim CS, Lu YH, Wang J, Xu J, et al. Nature. 2010; 463:1061–1065. [PubMed: 20182508]
[145]. Wang F, Liu XG. J. Am. Chem. Soc. 2008; 130:5642. + [PubMed: 18393419]
[146]. Zhu H, Ding Y.j. Wang AQ, Sun X, Wu XC, Zhu JJ. J. Mater. Chem. B. 2015; 3:458–464.
[147]. Ma D, Meng L, Chen Y, Hu M, Chen Y, Huang C, et al. ACS Appl. Mater. Interfaces. 2015; 7:16257–16265. [PubMed: 26161913]
[148]. Li Z, Liang T, Lv S, Zhuang Q, Liu Z. J. Am. Chem. Soc. 2015; 137:11179–11185. [PubMed: 26287332]
[149]. Bouzigues C, Gacoin T, Alexandrou A. ACS nano. 2011; 5:8488–8505. [PubMed: 21981700]
[150]. DaCosta MV, Doughan S, Han Y, Krull UJ. Anal. Chim. Acta. 2014; 832:1–33. [PubMed: 24890691]
[151]. Liu Y, Tu D, Zhu H, Chen X. Chem. Soc. Rev. 2013; 42:6924–6958. [PubMed: 23775339]
[152]. Dong H, Du SR, Zheng XY, Lyu GM, Sun LD, Li LD, et al. Chem. Rev. 2015; 115:10725–10815. [PubMed: 26151155]
[153]. Prodi L, Rampazzo E, Rastrelli F, Speghini A, Zaccheroni N. Chem. Soc. Rev. 2015; 44:4922–4952. [PubMed: 26090530]
[154]. Chen G, Qiu H, Prasad PN, Chen X. Chem. Rev. 2014; 114:5161–5214. [PubMed: 24605868]
[155]. Chen J, Zhao JX. Sensors. 2012; 12:2414–2435. [PubMed: 22736958]
[156]. Kumar M, Zhang P. Biosens. Bioelectron. 2010; 25:2431–2435. [PubMed: 20456935]
[157]. Saleh SM, Ali R, Wolfbeis OS. Chem. Eur. J. 2011; 17:14611–14617. [PubMed: 22106007]
[158]. Li X, Wu Y, Liu Y, Zou X, Yao L, Li F, Feng W. Nanoscale. 2014; 6:1020–1028. [PubMed: 24292453]
[159]. Liu C, Wang Z, Jia H, Li Z. Chem. Commun. 2011; 47:4661–4663.
[160]. Li H, Wang L. Analyst. 2013; 138:1589–1595. [PubMed: 23353928]

Author Manuscript Author Manuscript Author Manuscript Author Manuscript

[161]. Xu S, Xu S, Zhu Y, Xu W, Zhou P, Zhou C, Dong B, Song H. Nanoscale. 2014; 6:12573–12579. [PubMed: 25184968]
[162]. Zhang Y, Wu L, Tang Y, Su Y, Lv Y. Anal. Methods. 2014; 6:9073–9077.
[163]. Wu J, Qin Y. Sensor Actuat. B-Chem. 2014; 192:51–55.
[164]. Wu S, Duan N, Shi Z, Fang C, Wang Z. Talanta. 2014; 128:327–336. [PubMed: 25059168]
[165]. Jiang X, Meng G. J. Lumin. 2013; 135:227–231.
[166]. Zhang J, Li B, Zhang L, Jiang H. Chem. Commun. 2012; 48:4860–4862.
[167]. Li C, Liu J, Alonso S, Li F, Zhang Y. Nanoscale. 2012; 4:6065–6071. [PubMed: 22930418]
[168]. Liu B, Tan H, Chen Y. Anal. Chim. Acta. 2013; 761:178–185. [PubMed: 23312329]
[169]. Chen H, Ren J. Talanta. 2012; 99:404–408. [PubMed: 22967571]
[170]. Xie LX, Qin Y, Chen HY. Anal. Chem. 2012; 84:1969–1974. [PubMed: 22320710]
[171]. Ge X, Sun L, Ma B, Jin D, Dong L, Shi L, Li N, Chen H, Huang W. Nanoscale. 2015; 7:13877–13887. [PubMed: 26219919]
[172]. Liu Q, Peng J, Sun L, Li F. ACS nano. 2011; 5:8040–8048. [PubMed: 21899309]
[173]. Liu Y, Chen M, Cao T, Sun Y, Li C, Liu Q, et al. J. Am. Chem. Soc. 2013; 135:9869–9876. [PubMed: 23763640]
[174]. Peng J, Xu W, Teoh CL, Han S, Kim B, Samanta A, et al. J. Am. Chem. Soc. 2015; 137:2336–2342. [PubMed: 25626163]
[175]. Vázquez-González M, Carrillo-Carrion C. J. Biomed. Opt. 2014; 19:101503–101509. [PubMed: 24853041]
[176]. Lou Y, Zhao Y, Chen J, Zhu J-J. J. Mater. Chem. C. 2014; 2:595–613.
[177]. Wu P, Zhao T, Wang S, Hou X. Nanoscale. 2014; 6:43–64. [PubMed: 24270674]
[178]. Jing L, Ding K, Kershaw SV, Kempson IM, Rogach AL, Gao M. Adv. Mater. 2014; 26:6367–6386. [PubMed: 25178258]
[179]. Silvi S, Credi A. Chem. Soc. Rev. 2015; 44:4275–4289. [PubMed: 25912483]
[180]. Wu P, Hou X, Xu J-J, Chen H-Y. Chem. Rev. 2014; 114:11027–11059. [PubMed: 25297826]
[181]. Zhang JJ, Zheng TT, Cheng FF, Zhang JR, Zhu JJ. Anal. Chem. 2011; 83:7902–7909. [PubMed: 21888423]
[182]. Zhang JJ, Zheng TT, Cheng FF, Zhu JJ. Chem. Commun. 2011; 47:1178–1180.
[183]. Stanisavljevic M, Krizkova S, Vaculovicova M, Kizek R, Adam V. Biosens. Bioelectron. 2015; 74:562–574. [PubMed: 26188679]
[184]. Gui R, Jin H, Wang Z, Tan L. Coord. Chem. Rev. 2015; 296:91–124.
[185]. Kuo SY, Li HH, Wu PJ, Chen CP, Huang YC, Chan YH. Anal. Chem. 2015; 87:4765–4771. [PubMed: 25822074]
[186]. Shamirian A, Ghai A, Snee PT. Sensors. 2015; 15:13028–13051. [PubMed: 26053750]
[187]. Liu B, Zeng F, Wu G, Wu S. Analyst. 2012; 137:3717–3724. [PubMed: 22737682]
[188]. Lee H-L, Dhenadhayalan N, Lin K-C. RSC Adv. 2015; 5:4926–4933.
[189]. Chen Y, Rosenzweig Z. Anal. Chem. 2002; 74:5132–5138. [PubMed: 12380840]
[190]. Cai C, Cheng H, Wang Y, Bao H. RSC Adv. 2014; 4:59157–59163.
[191]. Wu P, Yan XP. Chem. Commun. 2010; 46:7046–7048.
[192]. Swarnkar A, Shanker GS, Nag A. Chem. Commun. 2014; 50:4743–4746.
[193]. Wu D, Chen Z, Huang G, Liu X. Sensors Actuat. A: Phys. 2014; 205:72–78.
[194]. Bu X, Zhou Y, He M, Chen Z, Zhang T. Dalton Trans. 2013; 42:15411–15420. [PubMed: 24013872]
[195]. Liang GX, Liu HY, Zhang JR, Zhu JJ. Talanta. 2010; 80:2172–2176. [PubMed: 20152468]
[196]. Sha J, Tong C, Zhang H, Feng L, Liu B, Lü C. Dyes Pigments. 2015; 113:102–109.
[197]. Ding Y, Shen SZ, Sun H, Sun K, Liu F. Sensors Actuat. B: Chem. 2014; 203:35–43.
[198]. Zhao X, Du J, Wu Y, Liu H, Hao X. J. Mater. Chem. A. 2013; 1:11748–11753.
[199]. Xie C, Xiao L, Peng S, Shi X. New J. Chem. 2014; 38:6095–6102.

Author Manuscript Author Manuscript Author Manuscript Author Manuscript

[200]. Yang P, Zhao Y, Lu Y, Xu QZ, Xu XW, Dong L, Yu SH. ACS nano. 2011; 5:2147–2154. [PubMed: 21344860]
[201]. Tao H, Liao X, Xu M, Li S, Zhong F, Yi Z. J. Lumin. 2014; 146:376–381.
[202]. Mu Q, Li Y, Xu H, Ma Y, Zhu W, Zhong X. Talanta. 2014; 119:564–571. [PubMed: 24401456]
[203]. Yuan C, Zhang K, Zhang Z, Wang S. Anal. Chem. 2012; 84:9792–9801. [PubMed: 23121315]
[204]. Li T, Zhou Y, Sun J, Tang D, Guo S, Ding X. Microchim. Acta. 2011; 175:113–119.
[205]. Page LE, Zhang X, Jawaid AM, Snee PT. Chem. Commun. 2011; 47:7773–7775.
[206]. Zhu X, Zhao Z, Chi X, Gao J. Analyst. 2013; 138:3230–3237. [PubMed: 23604099]
[207]. Freitas DV, Dias JMM, Passos SGB, de Souza GCS, Neto ET, Navarro M. Green Chem. 2014; 16:3247–3254.
[208]. Zhao Q, Rong X, Ma H, Tao G. J. Hazard. Mater. 2013; 250-251:45–52. [PubMed: 23434478]
[209]. de Souza GCS, de Santana ÉEA, da Silva PAB, Freitas DV, Navarro M, Paim APS, et al. Talanta. 2015; 144:986–991. [PubMed: 26452917]
[210]. Han J, Bu X, Zhou D, Zhang H, Yang B. RSC Adv. 2014; 4:32946–32952.
[211]. Li S, Chen D, Zheng F, Zhou H, Jiang S, Wu Y. Adv. Funct. Mater. 2014; 24:7133–7138.
[212]. Ge S, Zhang C, Zhu Y, Yu J, Zhang S. Analyst. 2010; 135:111–115. [PubMed: 20024189]
[213]. Mahapatra N, Panja S, Mandal A, Halder M. J. Mater. Chem. C. 2014; 2:7373–7384.
[214]. Volker J, Zhou X, Ma X, Flessau S, Lin H, Schmittel M, Mews A. Angew. Chem. Int. Ed. Engl. 2010; 49:6865–6868. [PubMed: 20715227]
[215]. Xia Y, Wang J, Zhang Y, Song L, Ye J, Yang G, Tan K. Nanoscale. 2012; 4:5954–5959. [PubMed: 22948544]
[216]. Wu C-S, Khaing Oo MK, Fan X. ACS nano. 2010; 4:5897–5904. [PubMed: 20925347]
[217]. Zhu H, Yu T, Xu H, Zhang K, Jiang H, Zhang Z, Wang Z, Wang S. ACS Appl. Mater. Interfaces. 2014; 6:21461–21467. [PubMed: 25354513]
[218]. Hao C, Xua L, Xing C, Kuang H, Wang L, Xu C. Biosens. Bioelectron. 2012; 36:174–178. [PubMed: 22560162]
[219]. Prasuhn DE, Feltz A, Blanco-Canosa JB, Susumu K, Stewart MH, Mei BC, et al. ACS nano. 2010; 4:5487–5497. [PubMed: 20822159]
[220]. Guo C, Wang J, Cheng J, Dai Z. Biosens. Bioelectron. 2012; 36:69–74. [PubMed: 22521943]
[221]. Hao Y, Liu L, Long Y, Wang J, Liu YN, Zhou F. Biosens. Bioelectron. 2013; 41:723–729. [PubMed: 23102430]
[222]. Hu B, Hu L-L, Chen M-L, Wang J-H. Biosens. Bioelectron. 2013; 49:499–505. [PubMed: 23811485]
[223]. Ma Q, Lin Z-H, Yang N, Li Y, Su X-G. Acta Biomater. 2014; 10:868–874. [PubMed: 24211611]
[224]. Xiong W-W, Yang G-H, Wu X-C, Zhu J-J. J. Mater. Chem. B. 2013; 1:4160.
[225]. Fu Y, Ding C, Zhu A, Deng Z, Tian Y, Jin M. Anal. Chem. 2013; 85:11936–11943. [PubMed: 24256150]
[226]. Wu L, Guo QS, Liu YQ, Sun QJ. Anal. Chem. 2015; 87:5318–5323. [PubMed: 25932651]
[227]. Wu P, Yan XP. Chem. Soc. Rev. 2013; 42:5489–5521. [PubMed: 23525298]
[228]. Dong Y, Choi J, Jeong HK, Son DH. J. Am. Chem. Soc. 2015; 137:5549–5554. [PubMed: 25860231]
[229]. Cao YC. Science. 2011; 332:48–49. [PubMed: 21454779]
[230]. Sarkar S, Maity AR, Karan NS, Pradhan N. J. Phys. Chem. C. 2013; 117:21988–21994.
[231]. Shang Y, Qi L, Wu F.-y. Microchim. Acta. 2012; 177:333–339.
[232]. Huang D, Niu C, Wang X, Lv X, Zeng G. Anal. Chem. 2013; 85:1164–1170. [PubMed: 23256544]
[233]. Leng X, Huang D, Niu C, Wang X, Zeng G, Niu Q. Anal. Methods. 2014; 6:6265–6270.
[234]. Jin Q, Hu Y, Sun Y, Li Y, Huo J, Zhao X. RSC Adv. 2015; 5:41555–41562.
[235]. Liu X, Zhan X-S, Wu F-Y, Ma L-H. Aust. J. Chem. 2015; 68:315–321.
[236]. Ke J, Li X, Zhao Q, Hou Y, Chen J. Sci. Rep. 2014; 4:5624. [PubMed: 25005836]
[237]. Ren HB, Wu BY, Chen JT, Yan XP. Anal. Chem. 2011; 83:8239–8244. [PubMed: 21913678]

Author Manuscript Author Manuscript Author Manuscript Author Manuscript

[238]. Zhai X, Gong Y, Yang W, Kang H, Zhang X. RSC Adv. 2015; 5:63458–63464.
[239]. Ge S, Lan F, Yu F, Yu J. New J. Chem. 2015; 39:2380–2395.
[240]. Esteves da Silva JCG, Gonçalves HMR. Trends Anal. Chem. 2011; 30:1327–1336.
[241]. Zong J, Yang X, Trinchi A, Hardin S, Cole I, Zhu Y, et al. Biosens. Bioelectron. 2014; 51:330–335. [PubMed: 23994615]
[242]. Ding C, Zhu A, Tian Y. Acc. Chem. Res. 2014; 47:20–30. [PubMed: 23911118]
[243]. Lu W, Qin X, Liu S, Chang G, Zhang Y, Luo Y, et al. Anal. Chem. 2012; 84:5351–5357. [PubMed: 22681704]
[244]. Guo Y, Wang Z, Shao H, Jiang X. Carbon. 2013; 52:583–589.
[245]. Kim Y, Jang G, Lee TS. ACS Appl. Mater. Interfaces. 2015; 7:15649–15657. [PubMed: 26112227]
[246]. Yuan C, Liu B, Liu F, Han M-Y, Zhang Z. Anal. Chem. 2014; 86:1123–1130. [PubMed: 24377316]
[247]. Cao B, Yuan C, Liu B, Jiang C, Guan G, Han MY. Anal. Chim. Acta. 2013; 786:146–152. [PubMed: 23790304]
[248]. Zhu A, Qu Q, Shao X, Kong B, Tian Y. Angew. Chem. Int. Ed. Engl. 2012; 51:7185–7189. [PubMed: 22407813]
[249]. Salinas-Castillo A, Ariza-Avidad M, Pritz C, Camprubi-Robles M, Fernandez B, Ruedas-Rama MJ. Chem. Commun. 2013; 49:1103–1105.
[250]. Li, L.-s.; Yan, X. J. Phys. Chem. Lett. 2010; 1:2572–2576.
[251]. Benítez-Martínez S, Valcárcel M. Trends Anal. Chem. 2015; 72:93–113.
[252]. Li L, Wu G, Yang G, Peng J, Zhao J, Zhu JJ. Nanoscale. 2013; 5:4015–4039. [PubMed: 23579482]
[253]. Suryawanshi A, Biswal M, Mhamane D, Gokhale R, Patil S, Guin D, Ogale S. Nanoscale. 2014; 6:11664–11670. [PubMed: 25162814]
[254]. Chakraborti H, Sinha S, Ghosh S, Pal SK. Mater Lett. 2013; 97:78–80.
[255]. Ha HD, Jang M-H, Liu F, Cho Y-H, Seo TS. Carbon. 2015; 81:367–375.
[256]. Sun X, Liu P, Wu L, Liu B. Analyst. 2015
[257]. Cai F, Liu XD, Liu S, Liu H, Huang YM. Rsc Adv. 2014; 4:52016–52022.
[258]. Huang H, Liao L, Xu X, Zou M, Liu F, Li N. Talanta. 2013; 117:152–157. [PubMed: 24209324]
[259]. Li S, Li Y, Cao J, Zhu J, Fan L, Li X. Anal. Chem. 2014; 86:10201–10207. [PubMed: 25280346]
[260]. Zhang Y-L, Wang L, Zhang H-C, Liu Y, Wang H-Y, Kang Z-H, Lee S-T. RSC Adv. 2013; 3:3733.
[261]. Li M, Zhou X, Ding W, Guo S, Wu N. Biosens. Bioelectron. 2013; 41:889–893. [PubMed: 23098856]
[262]. Liu F, Ha HD, Han DJ, Seo TS. Small. 2013; 9:3410–3414. [PubMed: 23606642]
[263]. Sun H, Gao N, Wu L, Ren J, Wei W, Qu X. Chem. Eur. J. 2013; 19:13362–13368. [PubMed: 23939943]
[264]. Wang, S.-e.; Si, S. Analy. Methods. 2013; 5:2947.
[265]. Zhang JJ, Liu Y, Hu LH, Jiang LP, Zhu JJ. Chem. Commun. 2011; 47:6551–6553.
[266]. Zhang L, Li T, Li B, Li J, Wang E. Chem. Commun. 2010; 46:1476–1478.
[267]. Li H, Zhai J, Sun X. Analyst. 2011; 136:2040–2043. [PubMed: 21442124]
[268]. Zhao C, Qu K, Song Y, Xu C, Ren J, Qu X. Chem. Eur. J. 2010; 16:8147–8154. [PubMed: 20512822]
[269]. Liu M, Zhang WQ, Chang DR, Zhang Q, Brennan JD, Li YF. Trend Anal. Chem. 2015; 74:120–129.
[270]. Liu M, Song JP, Shuang SM, Dong C, Brennan JD, Li YF. ACS nano. 2014; 8:5564–5573. [PubMed: 24857187]
[271]. He SJ, Song B, Li D, Zhu CF, Qi WP, Wen YQ, et al. Adv. Funct. Mater. 2010; 20:453–459.

Author Manuscript Author Manuscript Author Manuscript Author Manuscript

[272]. Ali MM, Aguirre SD, Lazim H, Li YF, et al. Angew. Chem. Int. Ed. Engl. 2011; 50:3751–3754. [PubMed: 21412961]

[273]. Tram K, Kanda P, Salena BJ, Huan SY, Li YF. Angew. Chem. Int. Ed. Engl. 2014; 53:12799–12802. [PubMed: 25213464]

[274]. Li D, Song SP, Fan CH. Acc. Chem. Res. 2010; 43:631–641. [PubMed: 20222738]

[275]. Pei H, Zuo XL, Zhu D, Huang Q, Fan CH. Acc. Chem. Res. 2014; 47:550–559. [PubMed: 24380626]

[276]. Lau PS, Coombes BK, Li YF. Angew. Chem. Int. Ed. Engl. 2010; 49:7938–7942. [PubMed: 20845339]

[277]. Tan W, Donovan MJ, Jiang J. Chem. Rev. 2013; 113:2842–2862. [PubMed: 23509854]

[278]. Lau PS, Li YF. Curr. Org. Chem. 2011; 15:557–575.

[279]. Zhang M, Yin BC, Tan W, Ye BC. Biosens. Bioelectron. 2011; 26:3260–3265. [PubMed: 21255996]

[280]. Wen Y, Xing F, He S, Song S, Wang L, Long Y, Li D, Fan C. Chem. Commun. 2010; 46:2596–2598.

[281]. Zhang JR, Huang WT, Xie WY, Wen T, Luo HQ, Li NB. Analyst. 2012; 137:3300–3305. [PubMed: 22655290]

[282]. Li X, Wang G, Ding X, Chen Y, Gou Y, Lu Y. Phys. Chem. Chem. Phys. 2013; 15:12800–12804. [PubMed: 23799396]

[283]. Mazumdar D, Liu J, Lu G, Zhou J, Lu Y. Chem. Commun. 2010; 46:1416–1418.

[284]. Lan T, Furuya K, Lu Y. Chem. Commun. 2010; 46:3896–3898.

[285]. Nelson KE, Ihms HE, Mazumdar D, Bruesehoff PJ, Lu Y. Chembiochem. 2012; 13:381–391. [PubMed: 22250000]

[286]. Ihms HE, Lu Y. Methods Mol. Biol. 2012; 848:297–316. [PubMed: 22315076]

[287]. Cepeda-Plaza M, Null EL, Lu Y. Nucleic Acids Res. 2013; 41:9361–9370. [PubMed: 23939617]

[288]. Zhang XB, Kong RM, Lu Y. Annu. Rev. Anal. Chem. 2011; 4:105–128.

[289]. He Y, Lu Y. Chem. Eur. J. 2011; 17:13732–13742. [PubMed: 22052817]

[290]. Li C, Wei L, Liu X, Lei L, Li G. Anal. Chim. Acta. 2014; 831:60–64. [PubMed: 24861972]

[291]. Yu Y, Liu Y, Zhen SJ, Huang CZ. Chem. Commun. 2013; 49:1942–1944.

[292]. Zhao XH, Kong RM, Zhang XB, Meng HM, Liu WN, Tan W, et al. Anal. Chem. 2011; 83:5062–5066. [PubMed: 21639104]

[293]. Liu M, Zhao H, Chen S, Yu H, Zhang Y, Quan X. Biosens. Bioelectron. 2011; 26:4111–4116. [PubMed: 21536425]

[294]. Wen Y, Peng C, Li D, Zhuo L, He S, Wang L, Huang Q, Xu QH, Fan C. Chem. Commun. 2011; 47:6278–6280.

[295]. Liu M, Zhao H, Chen S, Yu H, Zhang Y, Quan X. Chem. Commun. 2011; 47:7749–7751.

[296]. Wei W, Xu C, Ren J, Xu B, Qu X. Chem. Commun. 2012; 48:1284–1286.

Author Manuscript Author Manuscript Author Manuscript Author Manuscript

Research highlights

- New developments of the design and optical property of fluorescent nanoprobes are summarized.
- Recent advances in fluorescent nanoprobes-based sensing and imaging of metal ions both *in vitro* and *in vivo* are introduced.
- Future challenges and prospects of the application of fluorescent nanoprobes in living systems are concluded.

Author Manuscript Author Manuscript Author Manuscript Author Manuscript

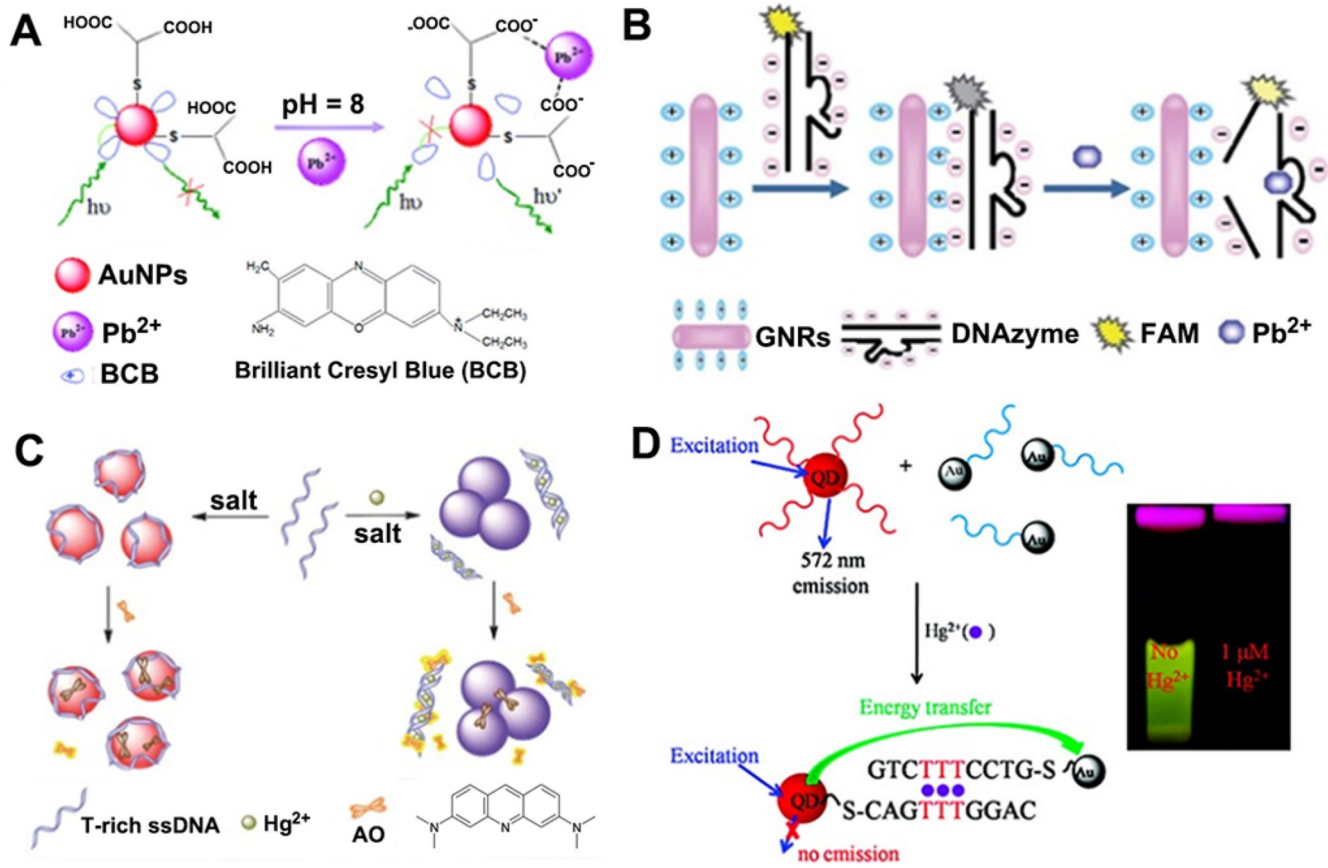

Figure 1.

(A) Illustration of the fluorescence resonance energy transfer (FRET)-based sensor of lead ions using brilliant cresyl blue (BCB) molecules as fluorophores. (B) The principle of Pb^{2+} detection by GNR-based FRET assay. (C) Schematic illustration of a label-free fluorescent sensor for Hg^{2+} detection based on acridine orange and aptamer-wrapped gold nanoparticles. (D) Schematic illustration of the operating principle of the QD/DNA/AuNP ensemble sensor for Hg^{2+} detection. (A: Adapted from [76] with permission of The Royal Society of Chemistry, B: Adapted from [86] by permission of The Royal Society of Chemistry, C: Adapted from [88] by permission of The Royal Society of Chemistry, D: Adapted with permission from [92]. Copyright 2011 American Chemical Society)

Author Manuscript Author Manuscript Author Manuscript Author Manuscript

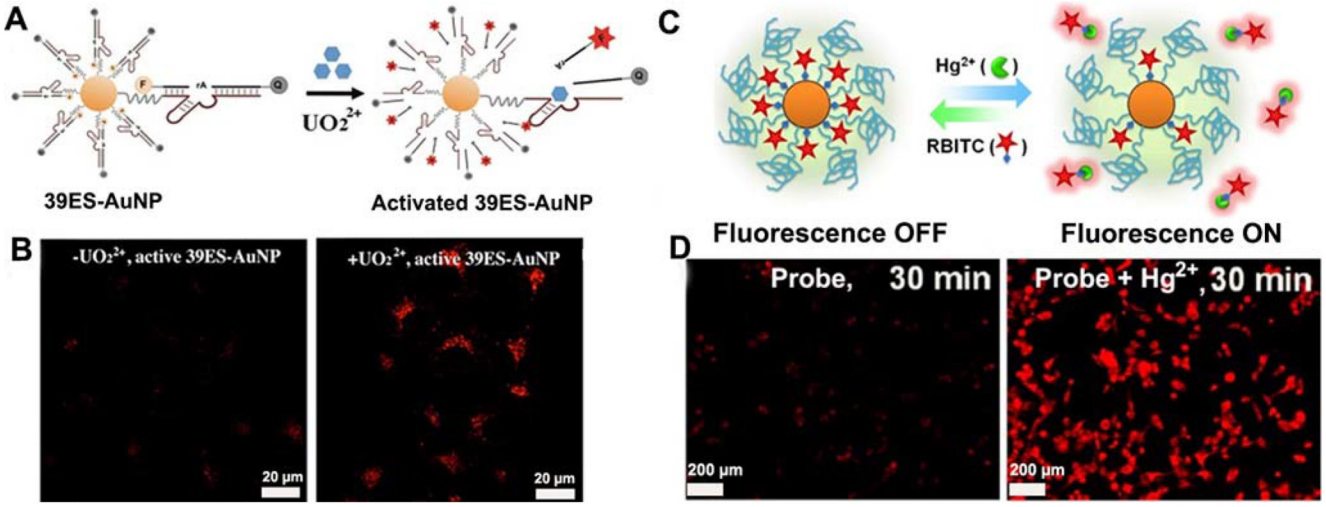

Figure 2.

(A) Design of a fluorescent DNAzyme immobilized onto gold nanoparticles as a selective probe of uranyl inside live cells. (B) Confocal microscopy images of HeLa cells treated with or without uranyl and incubated with active 39ES-AuNP (from left to right). (C) Schematic illustration of the design for detecting Hg^{2+} ions in a recyclable way. (D) Confocal microscopy images of MDA-MB-435 cells treated with or without 10 μM Hg^{2+} and incubated with 20 nM RBITC-PEG-AuNPs probe. (A and B: Adapted with permission from [95]. Copyright 2013 American Chemical Society, C and D: Adapted with permission from [96]. Copyright 2012 American Chemical Society)

Author Manuscript Author Manuscript Author Manuscript Author Manuscript

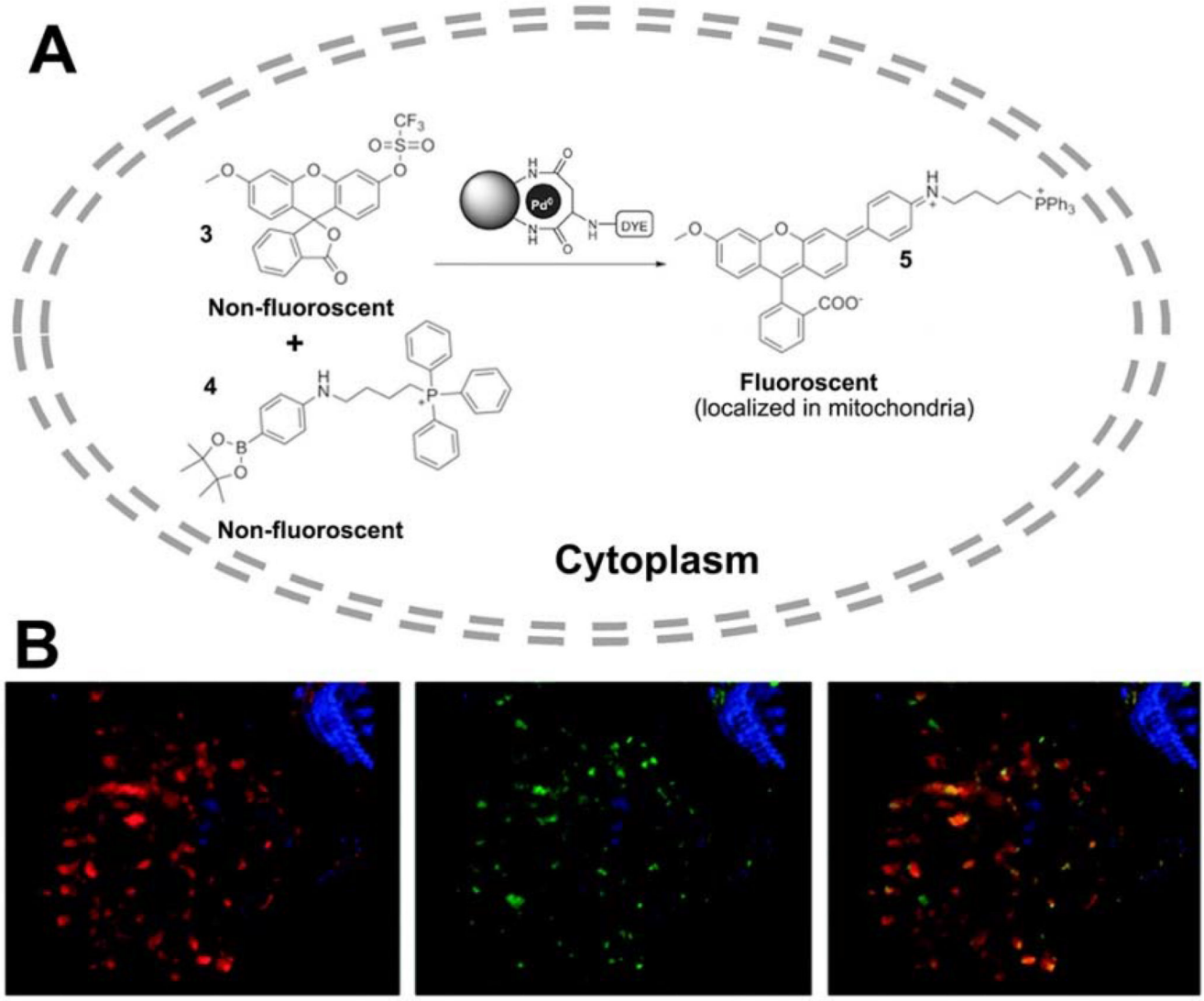

Figure 3.

(A) Pd^0-catalyzed intracellular cross-coupling of reagents 3 and 4 generates the mitochondria-localized fluorescent compound 5. (B) Deconvolved confocal images of a single cell showing co-localization of MitoTracker-labelled mitochondria and Suzuki–Miyaura product 5. Left panel: cell nucleus (blue) and mitochondria (red). Centre panel: cell nucleus (blue) and *in cellulo* synthesized compound 5 (green). Right panel: merged image (orange indicates co-localization). (Adapted with permission from [98]. Copyright 2011 *Nature*)

Author Manuscript Author Manuscript Author Manuscript Author Manuscript

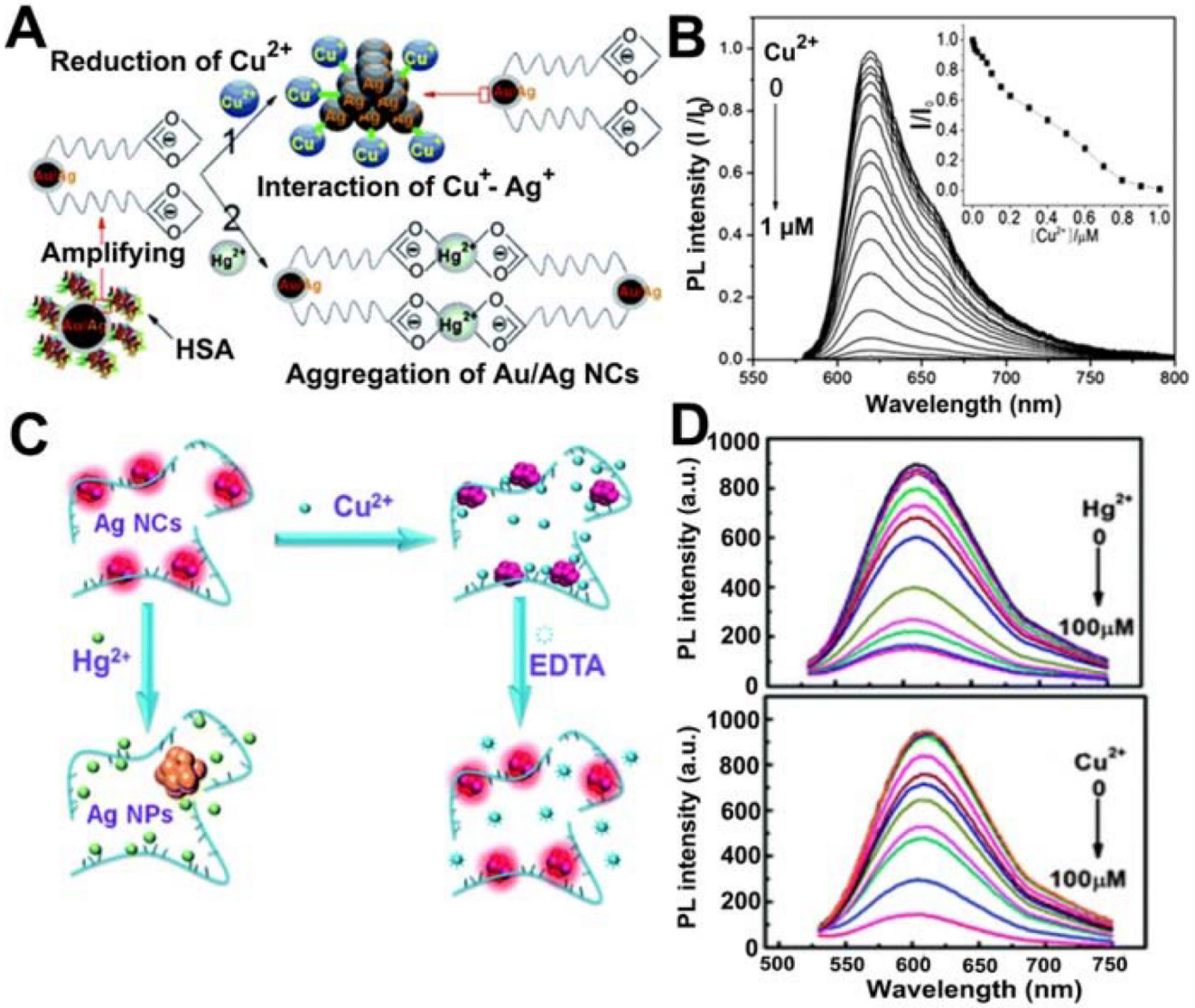

Figure 4.

(A) Schematic representation of the PL quenching mechanism of HSA-stabilized Au/Ag NCs by the addition of Cu^{2+} and Hg^{2+} ions (left), and PL emission spectra of Au/Ag NCs for Cu^{2+} detection (right). (B) Scheme of the mechanism of the detection of Hg^{2+}/Cu^{2+} by the AgNCs (left), and fluorescence changes of the Ag NCs (right) in the presence of different concentrations of Hg^{2+} (top) and Cu^{2+} (bottom). (A: Adapted from [110] with permission of The Royal Society of Chemistry, B: Adapted from [124] with permission of The Royal Society of Chemistry)

Author Manuscript Author Manuscript Author Manuscript Author Manuscript

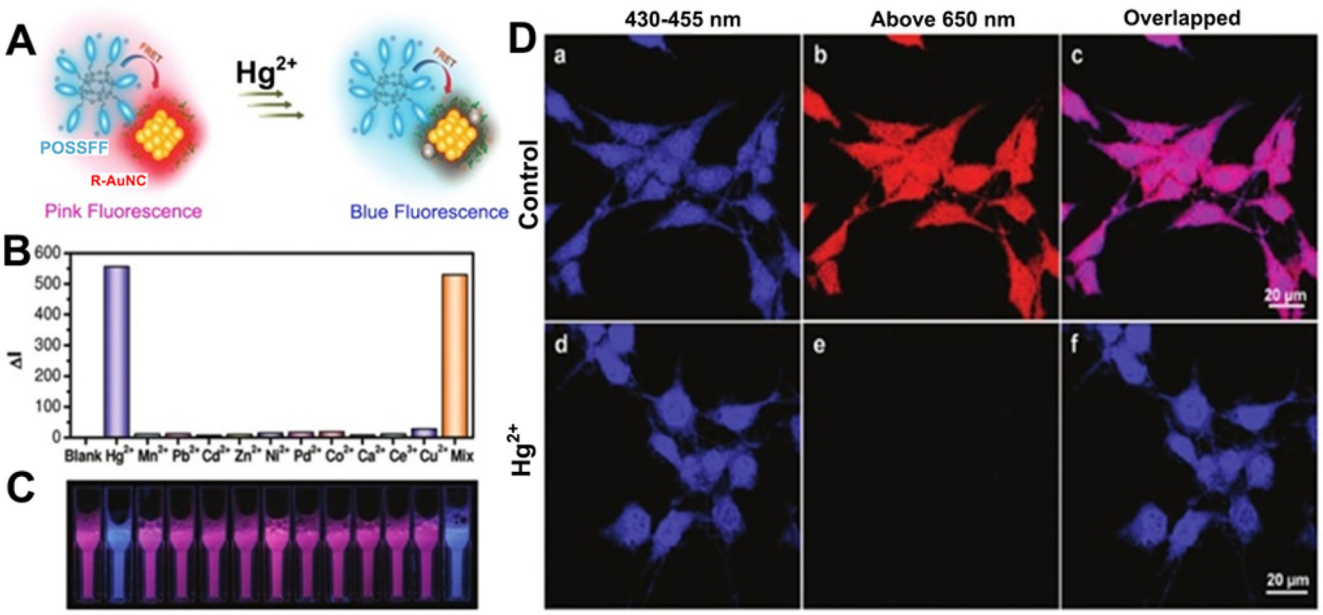

Figure 5.

(A) Schematic illustration of the visual detection of mercury ions based on FRET between POSSFF and R-AuNC. (B) ΔI for POSSFF/R-AuNC complex (15 mM, pH 7.4) as a function of metal ion species. (C) Photographs of the corresponding fluorescent solutions of POSSFF/R-AuNC complex in the absence and presence of metal ions under UV radiation at 365 nm. (D) CLSM fluorescence images of MCF-7 cells stained by POSSFF/R-AuNC complex in the (a-c) and (d-f) presence of Hg^{2+}. Excitation wavelength was at 405 nm. (Adapted with permission from [138]. Copyright 2011 American Chemical Society).

Author Manuscript Author Manuscript Author Manuscript Author Manuscript

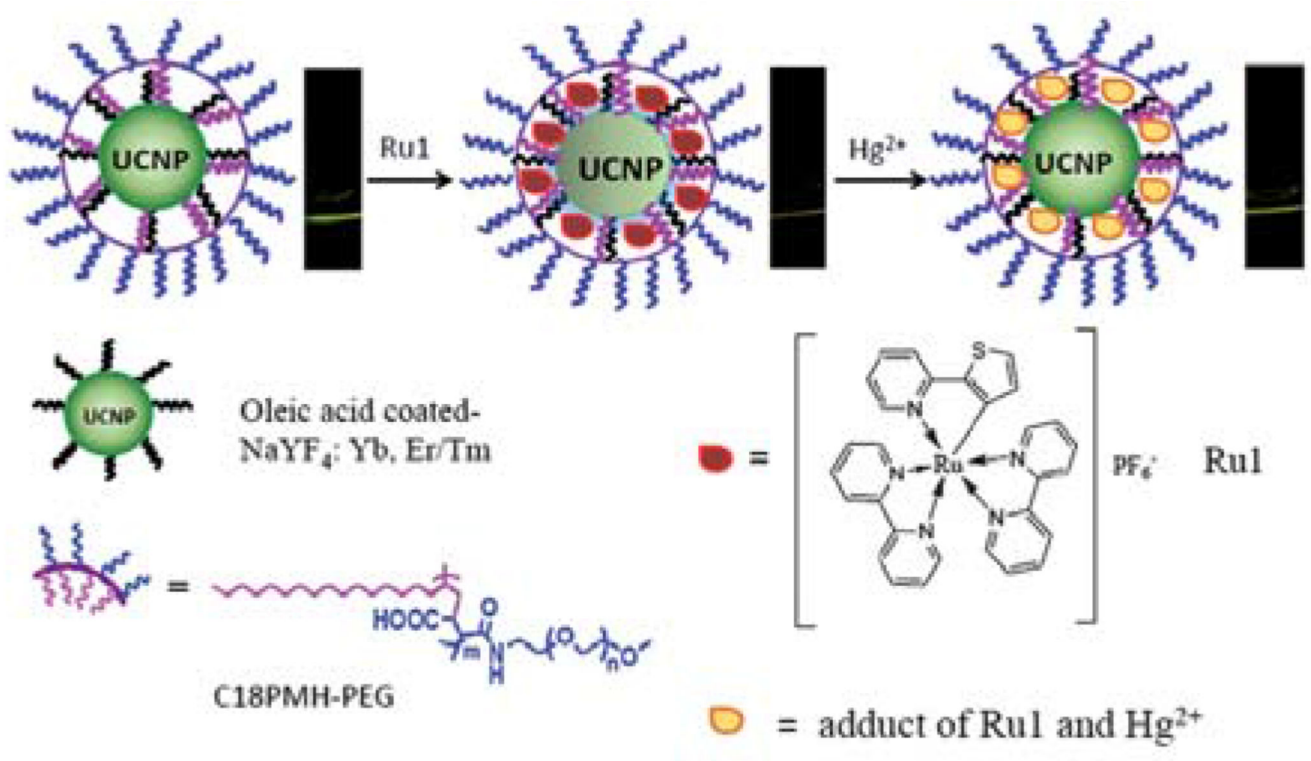

Figure 6.

Schematic illustration of the synthesis of a UCNP-based system and its application in upconversion luminescence detection of Hg^{2+}. (Adapted from [158] with permission of The Royal Society of Chemistry)

Author Manuscript Author Manuscript Author Manuscript Author Manuscript

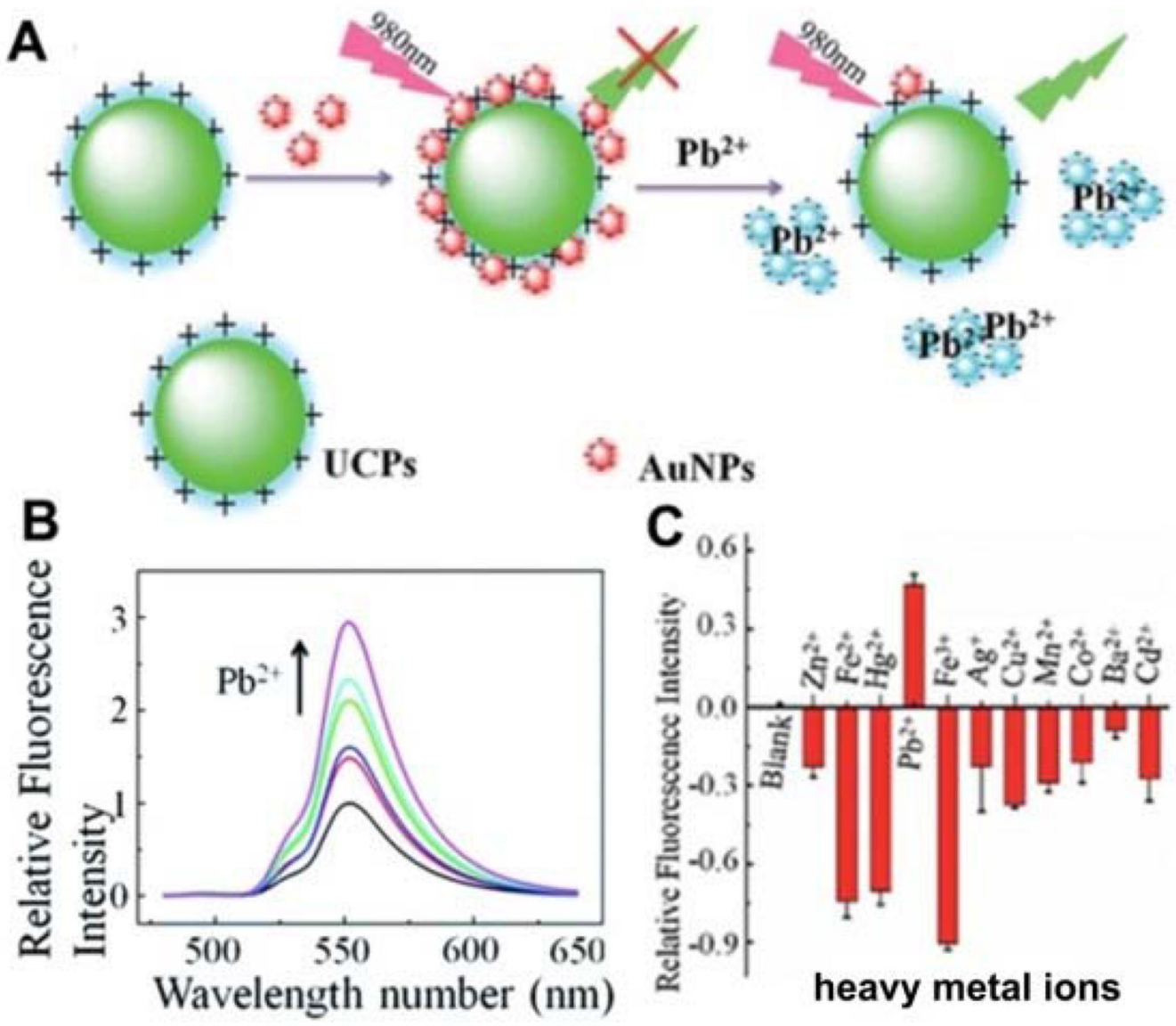

Figure 7.

(A) Schematic illustration of Pb^{2+} detection. (B) Evolution of UCP–AuNP fluorescence restoration with increasing concentrations of Pb^{2+}. (C) Fluorescence responses of UCP–AuNP to Pb^{2+} and a number of heavy metal ions (2.5 mM). (Adapted from [162] with permission of The Royal Society of Chemistry)

Author Manuscript Author Manuscript Author Manuscript Author Manuscript

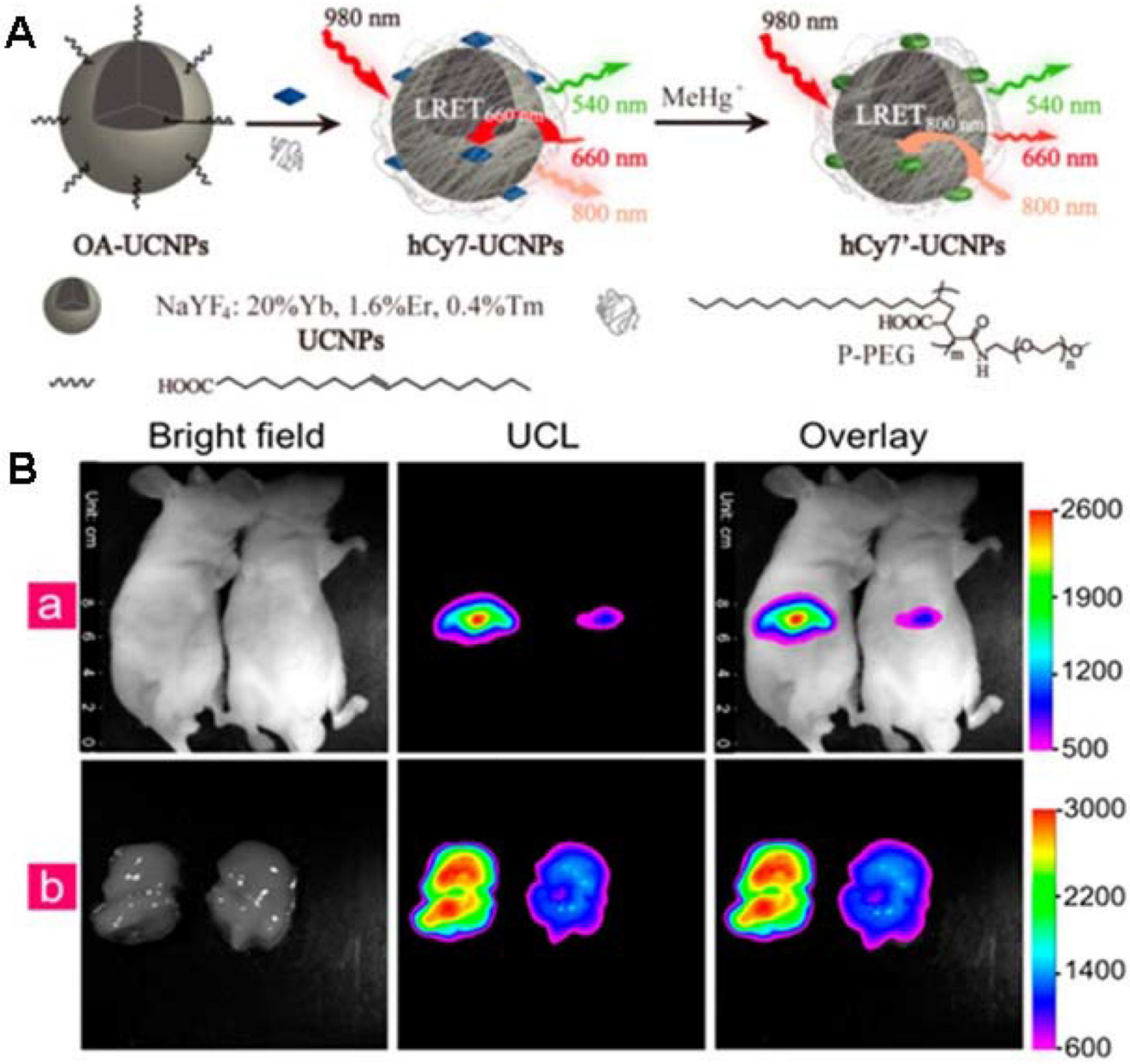

Figure 8.

(A) Schematic illustration of the synthesis of UCNPs hCy7 and its sensing to $MeHg^+$ with a change in UCL emission. (B) (a) *In vivo* UCL images of 40 μg hCy7-UCNPs-pretreated living mice injected intravenously with 0.2 mL normal saline (left mouse) or 0.1 mM $MeHg^+$ solution (right mouse). (b) The corresponding UCL images of the livers which were isolated from the above dissected mice. The UCL emission was collected at 800 ± 12 nm upon irradiation at 980 nm. (Adapted with permission from [173]. Copyright 2013 American Chemical Society.)

Author Manuscript Author Manuscript Author Manuscript Author Manuscript

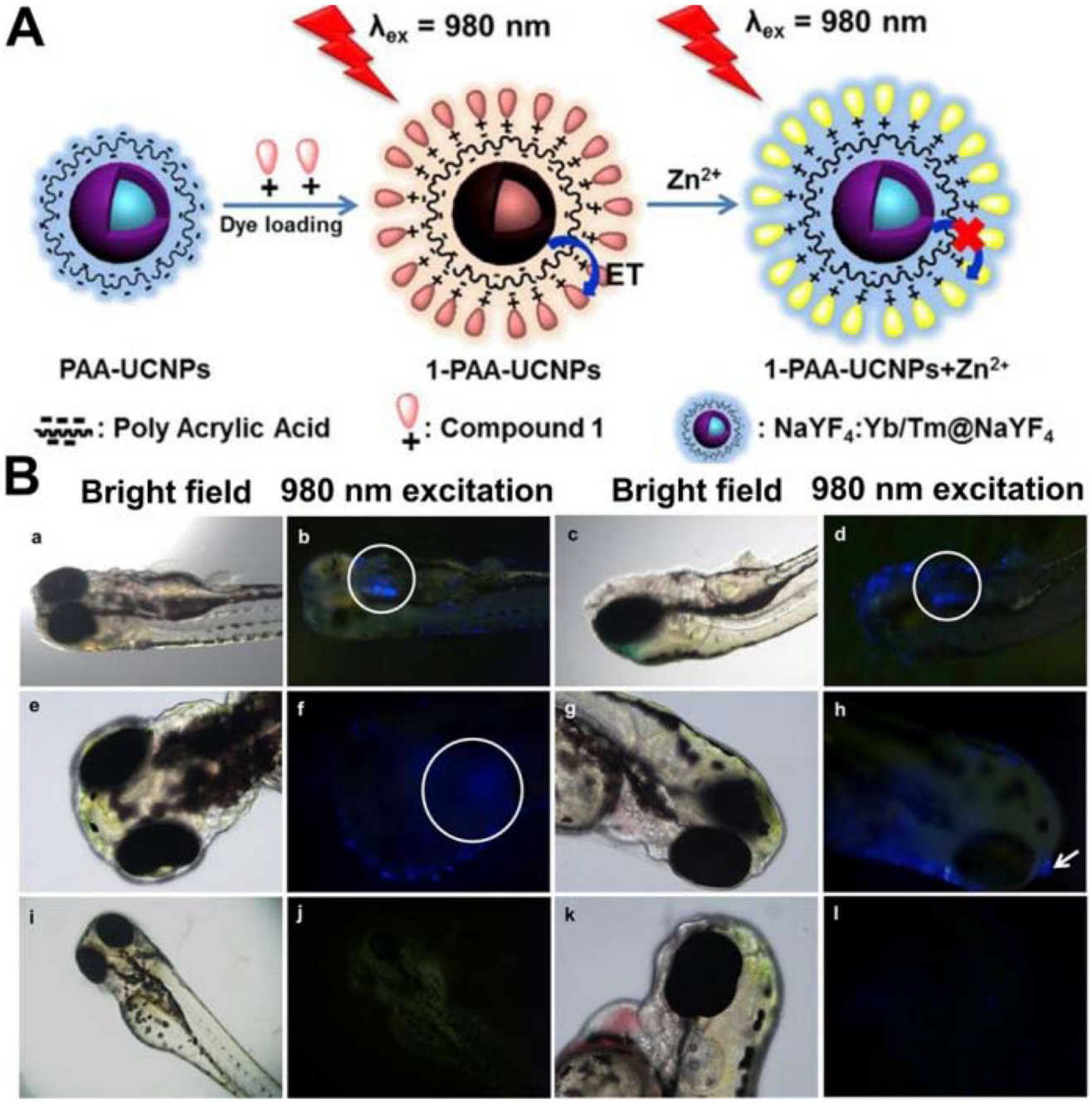

Figure 9.

(a) Schematic illustration showing the synthesis of chromophore-assembled UCNPs and their response to Zn^{2+}. (b) In vivo tracing distribution of Zn^{2+} in zebrafish. (Adapted with permission from [174]. Copyright 2015 American Chemical Society)

Author Manuscript Author Manuscript Author Manuscript Author Manuscript

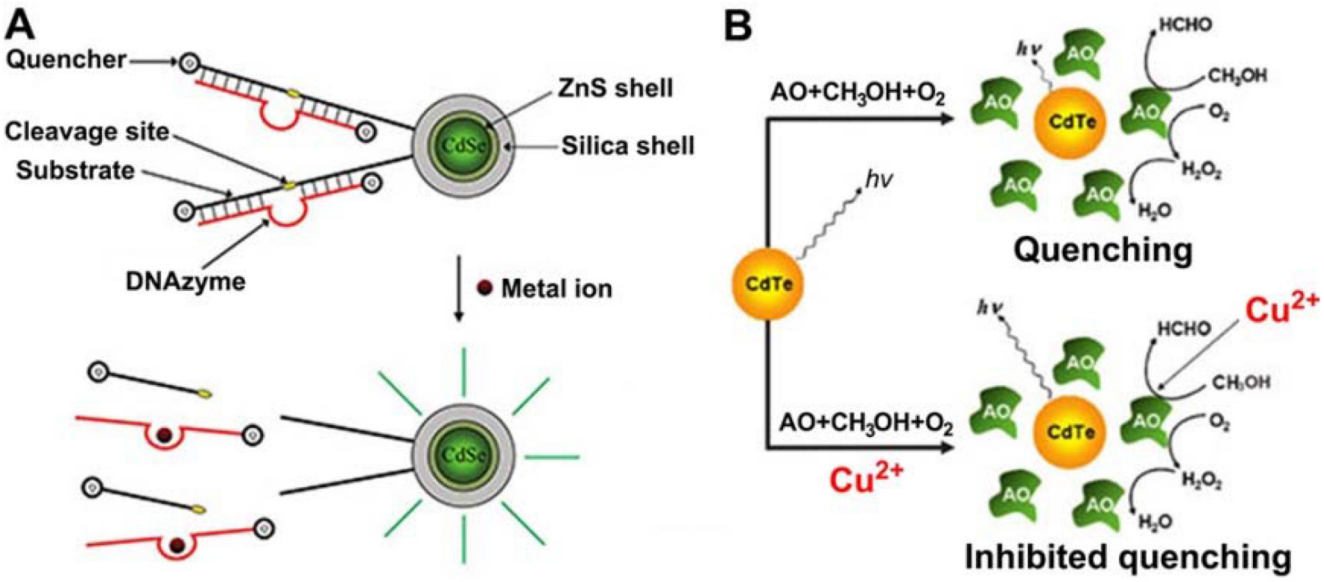

Figure 10.

(A) Schematic of the nanosensor based on QDs and DNAzymes for heavy metal ion detection. (B) Schematic representation of the activity of alcohol oxidase by the PL intensity of CdTe QDs, and its inhibition by copper ions. (A: Adapted with permission from [216]. Copyright 2010 American Chemical Society, (B): Adapted from [220] with permission from Elsevier)

Author Manuscript Author Manuscript Author Manuscript Author Manuscript

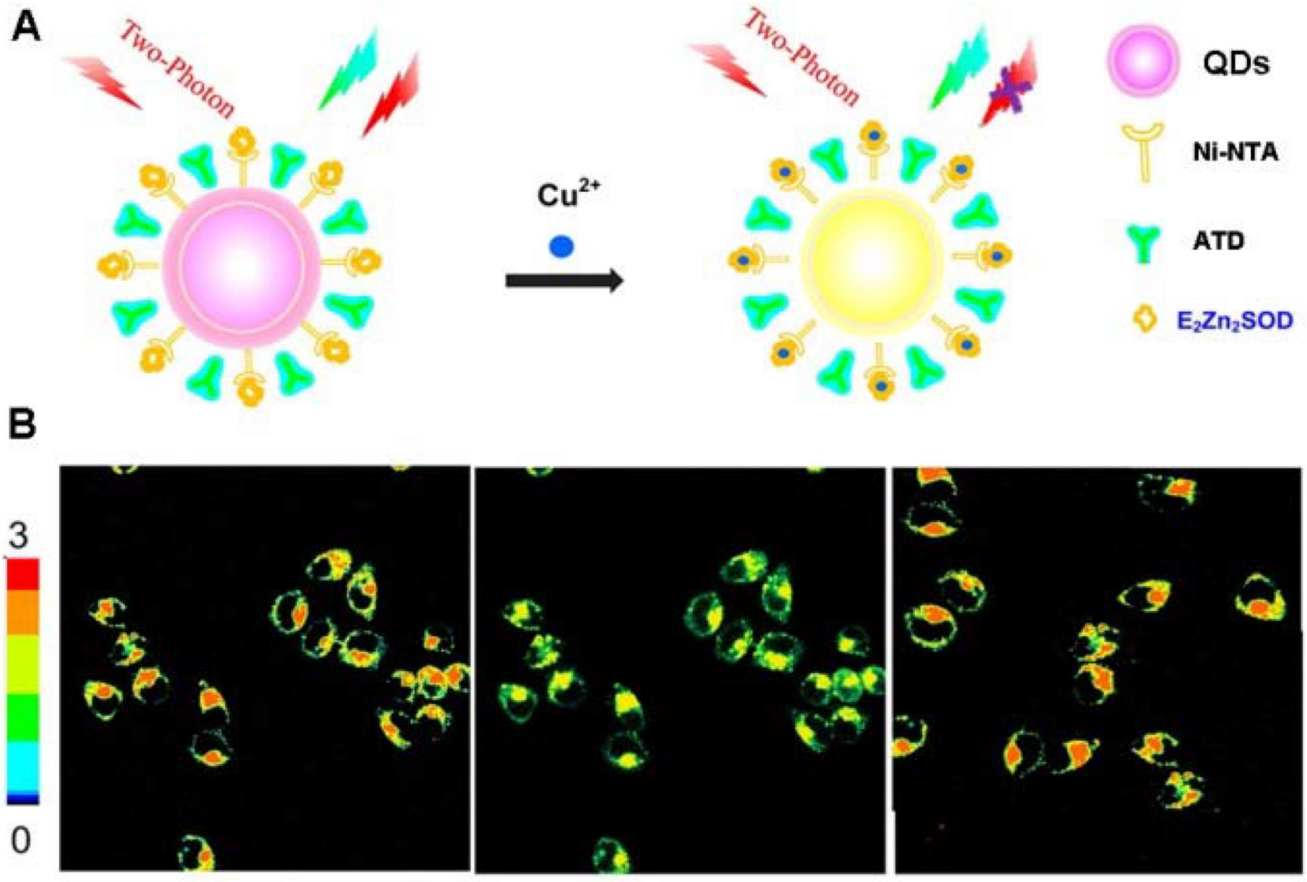

Figure 11.

(A) Schematic Illustration for the Working Principle of Two-Photon Ratiometric Imaging and Sensing of Cu^{2+}. (B) Two-photon ratiometric images of HeLa cells after treatment with 50 μM $CuCl_2$, 100 mM $CuCl_2$ for 1 h, followed by treatment with 100 mM EDTA for 0.5 h (from left to right). (Adapted with permission from [225]. Copyright 2013 American Chemical Society)

Author Manuscript Author Manuscript Author Manuscript Author Manuscript

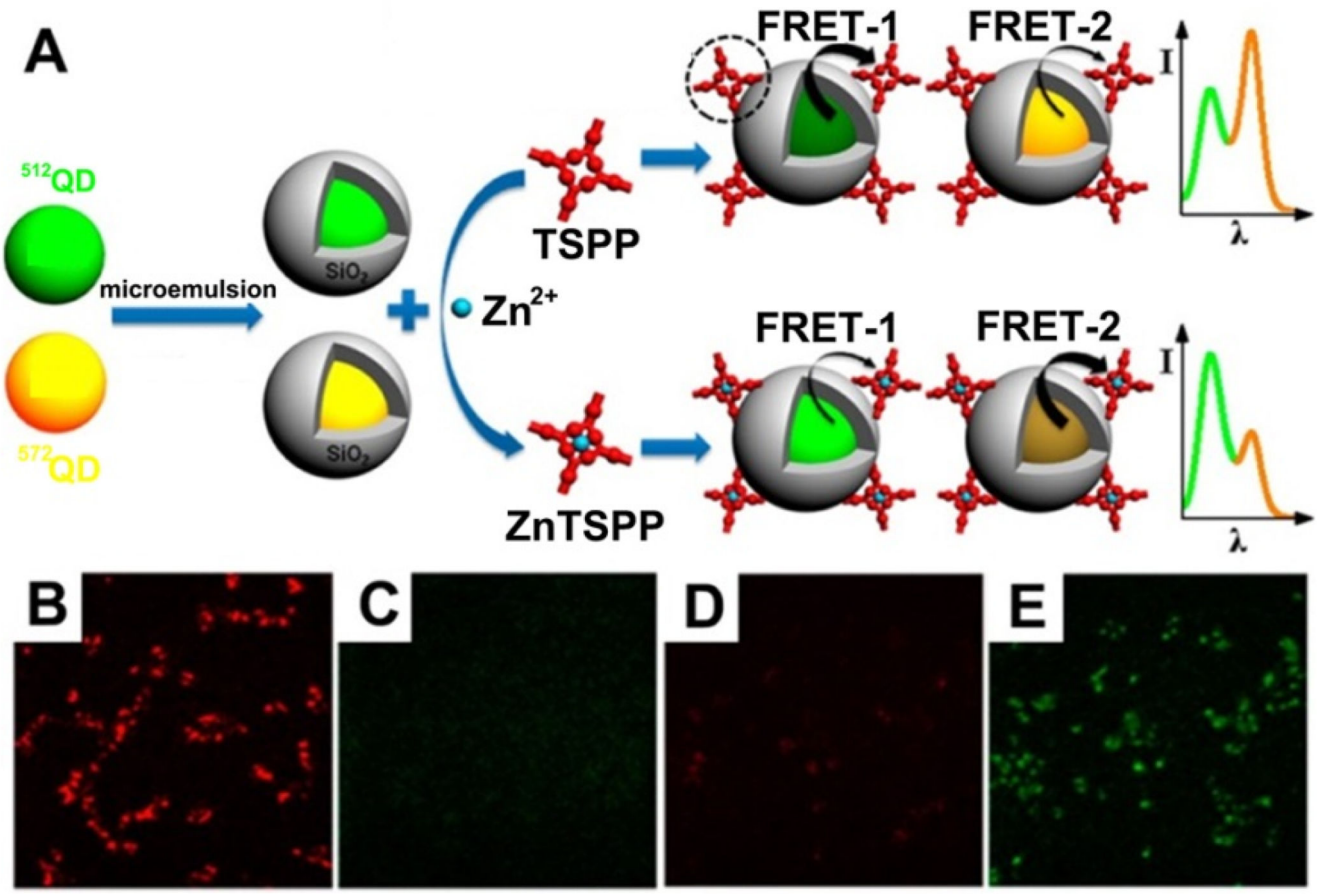

Figure 12.

Schematic illustration of the preparation and application of a dual-colored QD-based ratiometric fluorescent probe for the detection of Zn^{2+} (A). Fluorescent images of live HCT116 cells incubated with the probe, with (B, yellow channel, C, green channel) and without Zn^{2+} (D, yellow channel, E, green channel). (Adapted with permission from [226]. Copyright 2015 American Chemical Society)

Author Manuscript Author Manuscript Author Manuscript Author Manuscript

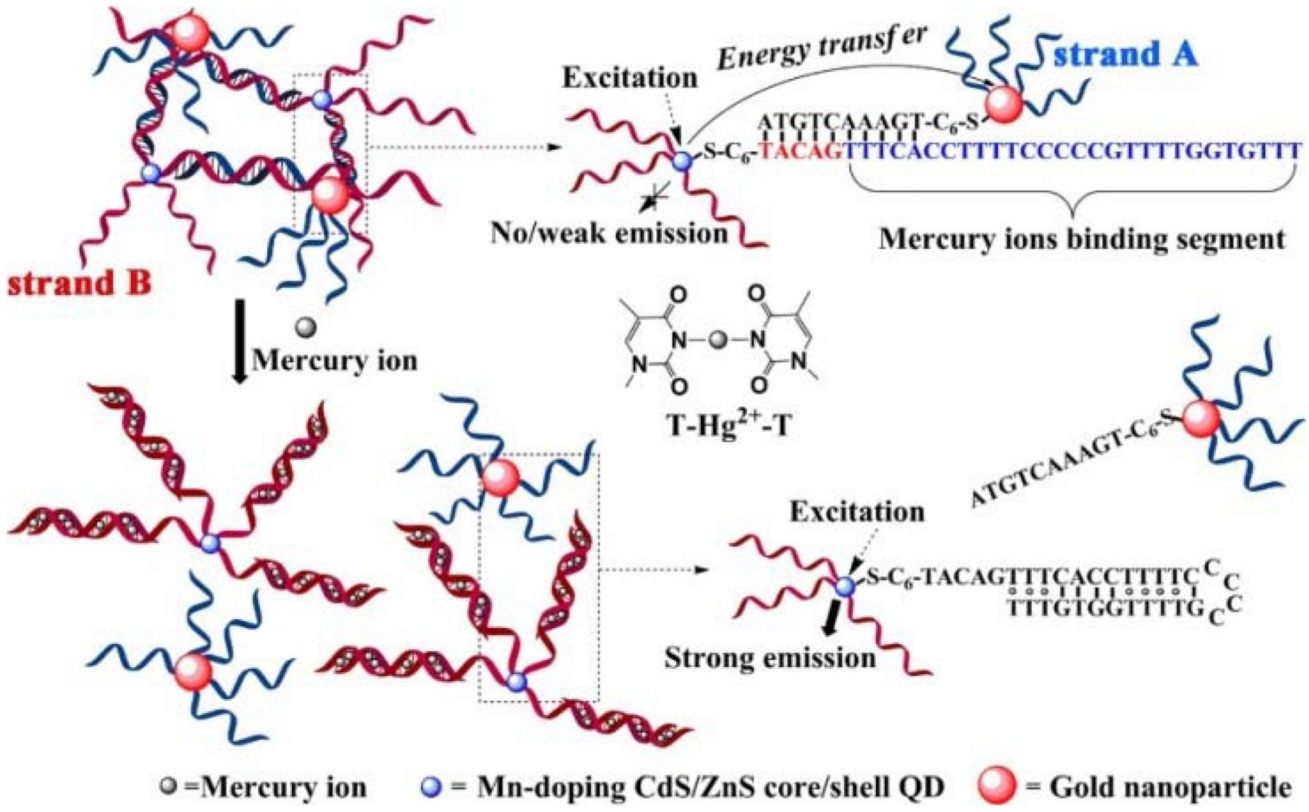

Figure 13.

Schematic description of the “turn-on” fluorescent sensor for Hg^{2+} based on the Hg^{2+}-mediated formation of DNA duplexes. (Adapted with permission from [232]. Copyright 2013 American Chemical Society.)

Author Manuscript Author Manuscript Author Manuscript Author Manuscript

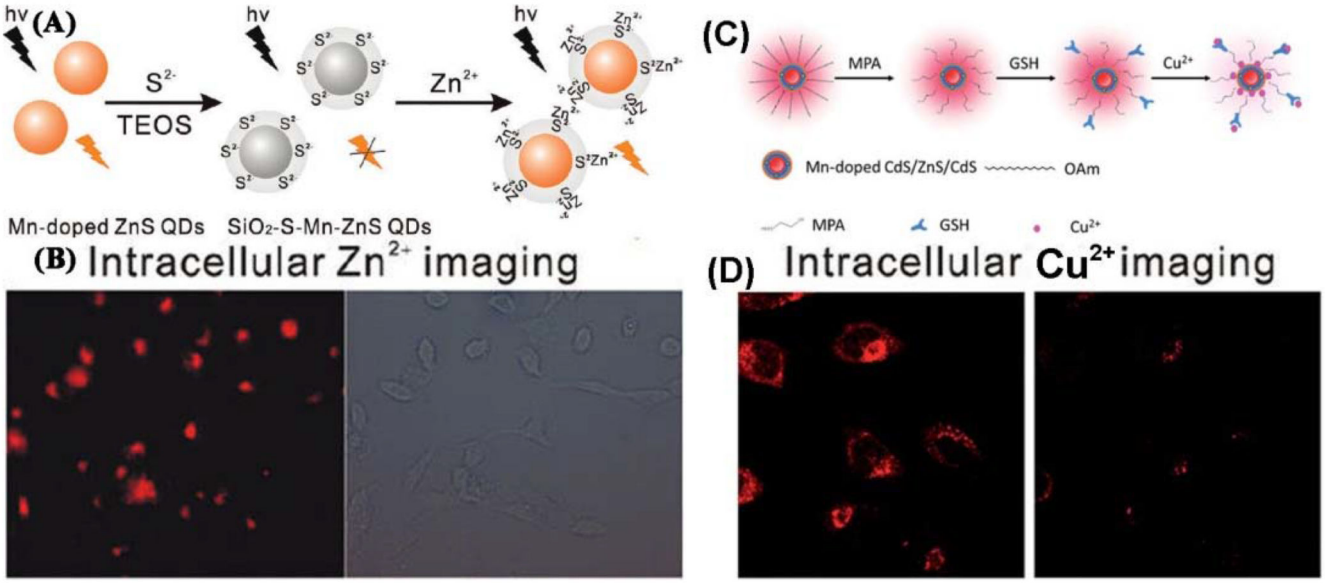

Figure 14.

(A) Schematic illustration for the fabrication of SiO_2-S-Mn-ZnS QDs as a turn-on PL probe for Zn^{2+}. (B) Intracellular imaging of Zn^{2+} with SiO_2-S-Mn-ZnS QDs. HepG2 cells were incubated with Zn^{2+} in a fresh serum-containing medium for 20h. The collected Zn^{2+}-uptaken HepG2 cells were then incubated with SiO_2-S-Mn-ZnS QDs in a fresh serum-free medium for 4h and then in a fresh serum containing medium for 12h. (C) Schematic illustration for the formation of GSH-capped Mn-doped CdS/ZnS/CdS QD-based fluorescent nanosensor for Cu^{2+}. (D). Confocal fluorescent images of HeLa cells before (left) and after (right) addition of Cu^{2+} (20 μM). (A and B: Adapted with permission from [237]. Copyright 2011 American Chemical Society, C and D: Adapted from [238] with permission of The Royal Society of Chemistry)

Author Manuscript Author Manuscript Author Manuscript Author Manuscript

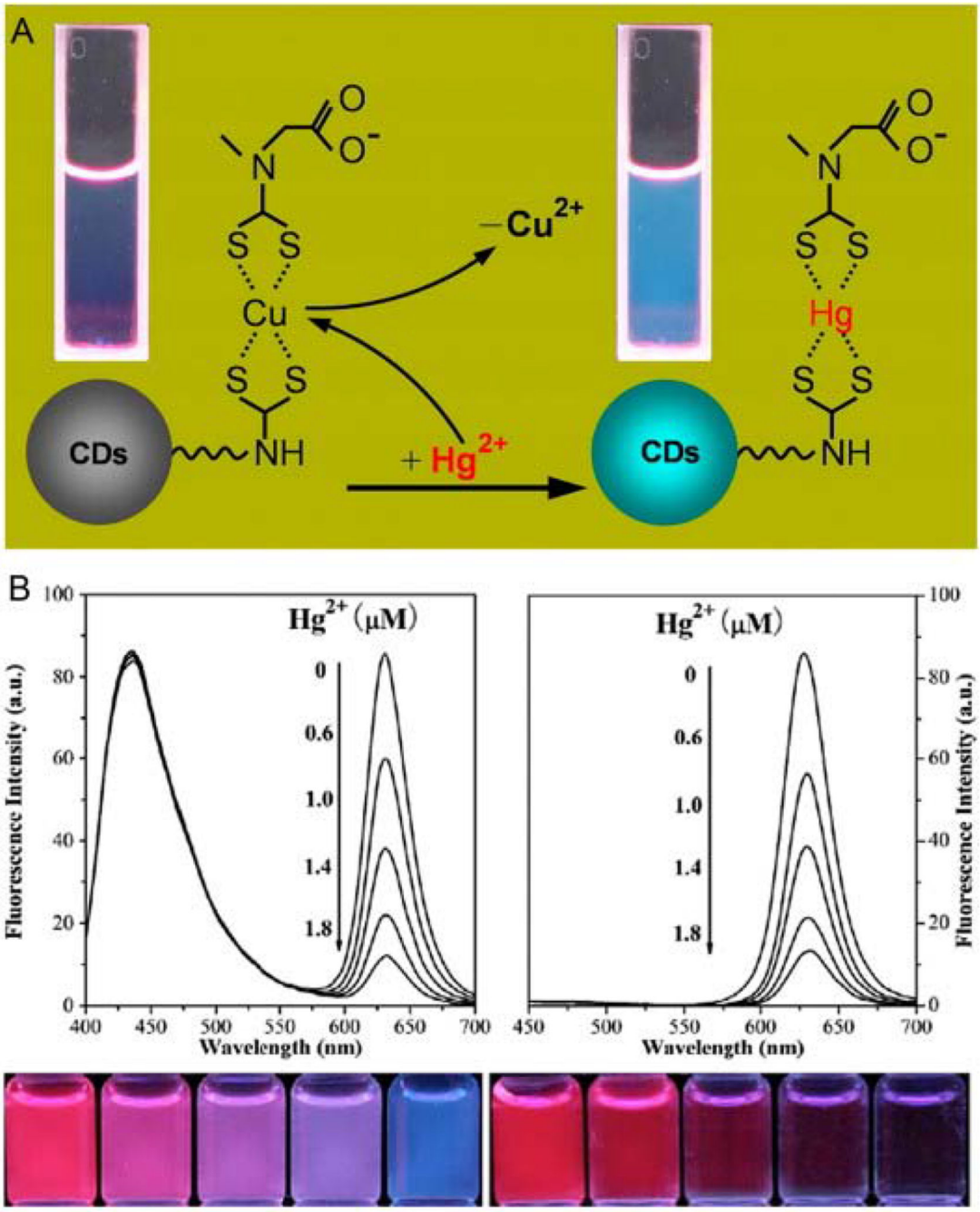

Figure 15.

(A) Fluorescence turn-on for the detection of Hg^{2+} with $CuDTC_2$ modified CNPs. (B) Ratiometric fluorescence detection of Hg^{2+} based on the hybrid of F-CNPs and QDs. (A: Adapted with permission from [246]. Copyright 2014 American Chemical Society, B: Adapted from [247] with permission of Elsevier).

Author Manuscript Author Manuscript Author Manuscript Author Manuscript

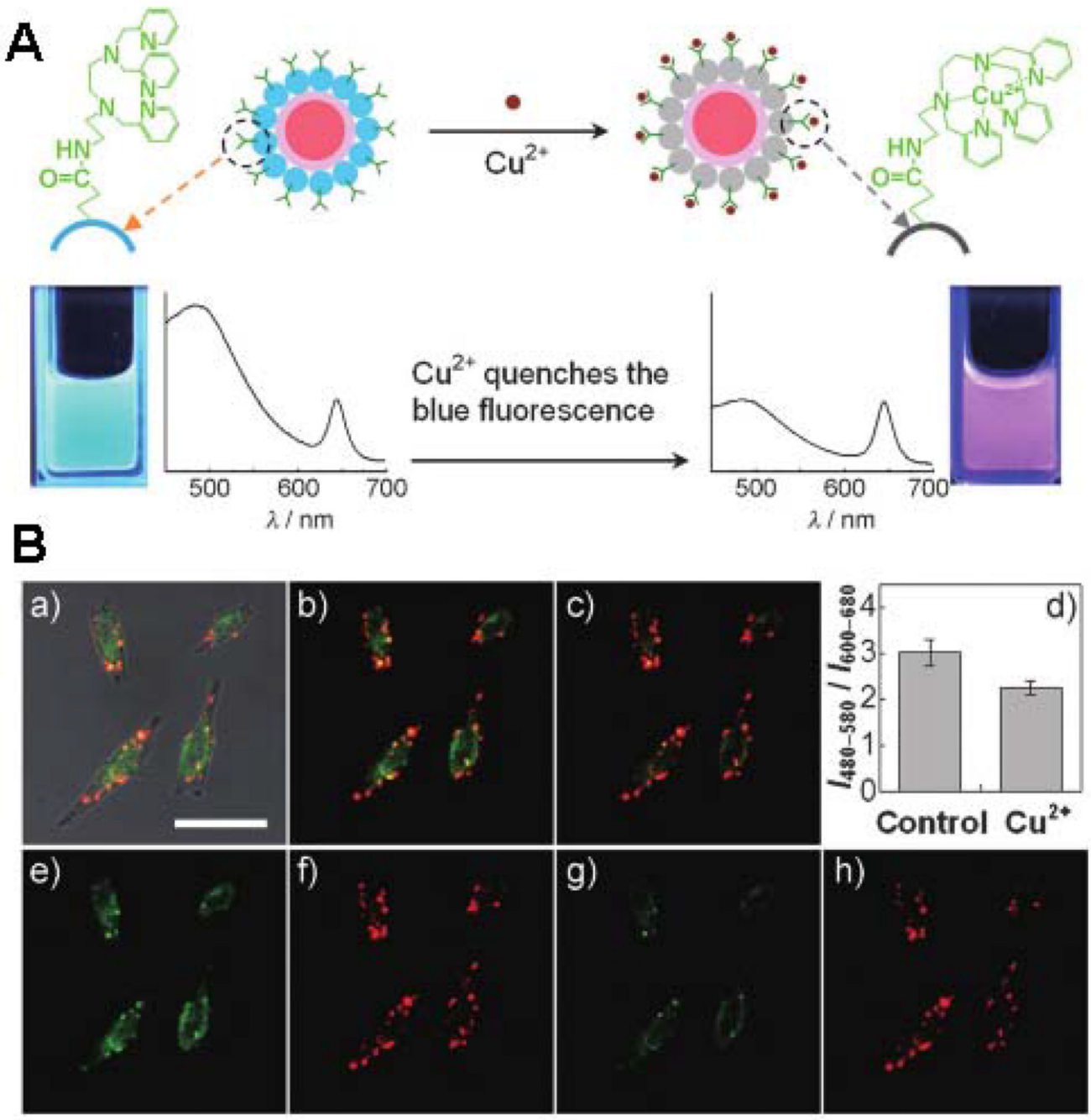

Figure 16.

(A) Schematic illustration of the dual-emission fluorescent sensing of Cu^{2+} based on CdSe@C-TPEA hybrid. (B) (a) The overlay of bright-field and fluorescence images of HeLa cells incubated with CdSe@C-TPEA. (b, c) Confocal fluorescence images of HeLa cells (b) before and (c) after the exogenous Cu2+ source treatment. (d) Bar graph representing the integrated intensity from 480 to 580 nm over the integrated fluorescence intensity from 600 to 680 nm; values are the mean ratio generated from the intensity from three randomly selected fields in both channel. (e, g) Confocal fluorescence images obtained from the

480-580 nm channel before and after the exogenous Cu^{2+} source treatment, while (f, h) are from the 600-680 channel. Scale Bar: 25 μm. (Reprinted with permission from [248]. Copyrights 2012 Wiley-VCH Verlag GmbH & Co. KGaA, Weinheim)

Author Manuscript Author Manuscript Author Manuscript Author Manuscript

Author Manuscript Author Manuscript Author Manuscript Author Manuscript

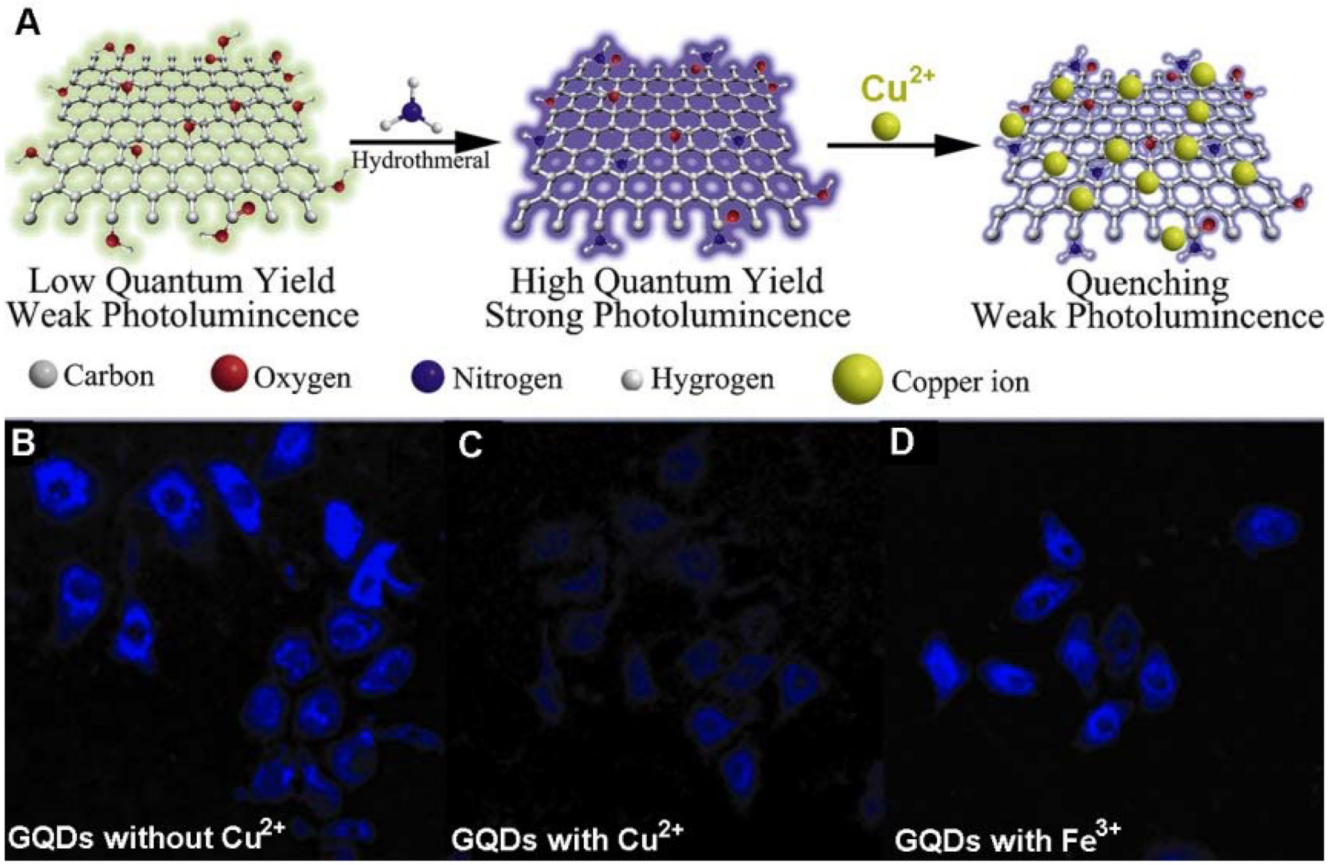

Figure 17.

Schematic representation of the preparation route for afGQDs, its quenching by copper ions, and intracellular Cu^{2+} profiling with afGQDs stained cells imaged without Cu^{2+} (B), with 10 μM Cu^{2+} (C), and with 10 μM Fe^{3+} (D) in dark field. (Reprinted with permission from [263]. Copyrights 2013 Wiley-VCH)

Author Manuscript Author Manuscript Author Manuscript Author Manuscript

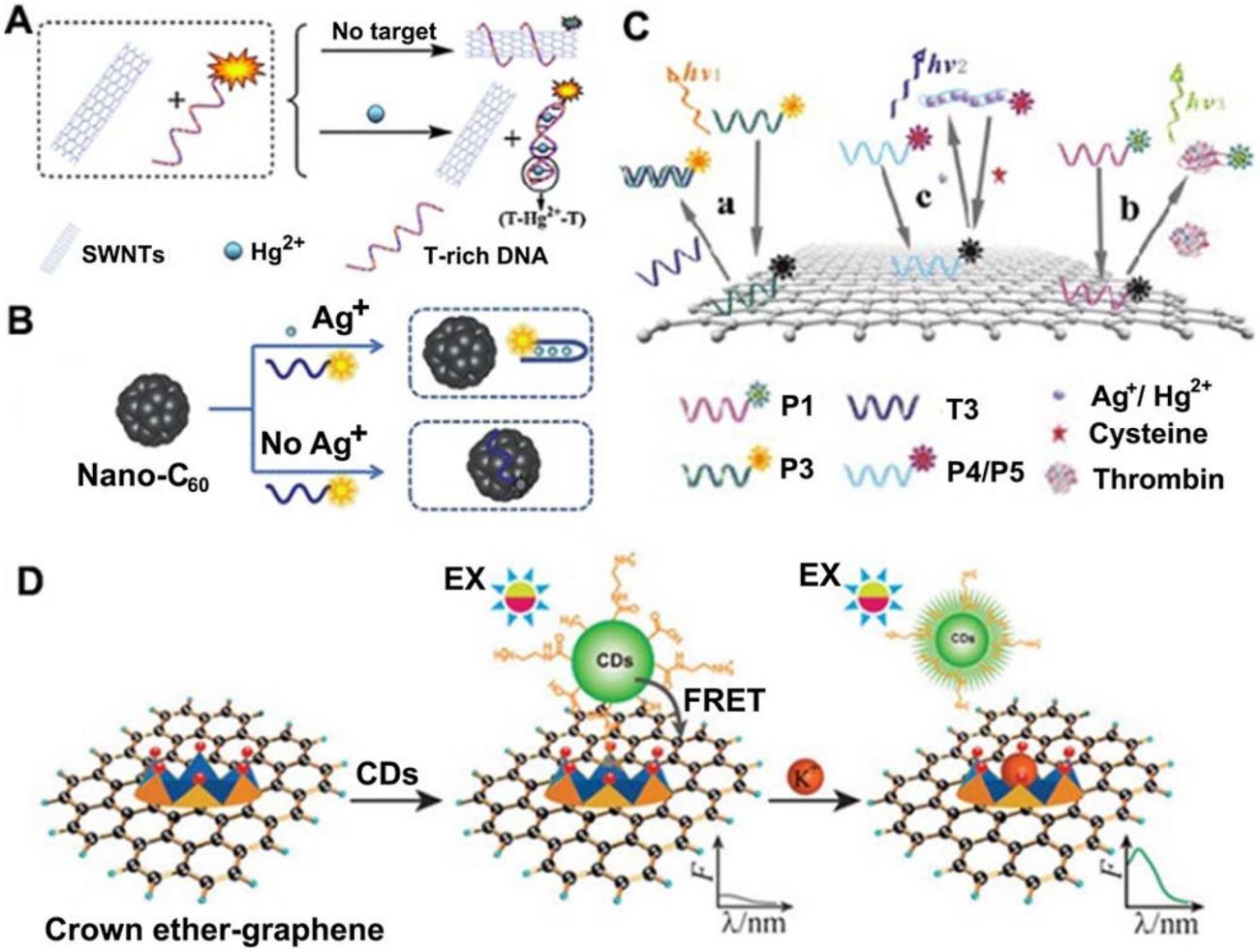

Figure 18.

(A) Schematic description of fluorescent sensing of Hg^{2+} based on the SWNTs and T-rich DNA. (B) A schematic to illustrate the nano-C60-based fluorescent Ag^{+} detection based on conformational change of an Ag^{+}- specific C-rich OND. (C) Schematic representation of the ssDNA–GO architecture platform for multiplex target detection. (D) Schematic illustration of the FRET model based on CDs–graphene and the mechanism of K+ determination. (A: Adapted from [266] with permission of The Royal Society of Chemistry, B: Adapted from [267] with permission of The Royal Society of Chemistry, C: Adapted from [279] with permission of Elsevier, D: Adapted from [296] with permission of The Royal Society of Chemistry)

Author Manuscript Author Manuscript Author Manuscript Author Manuscript

Table 1

Summary of representative reports of fluorescent nanoprobes for metal ions sensing.

Type of nanomaterials[a]		Analytes	Detection mechanism[a]	Detection limit	Reference
Noble metal nanomaterials	Metal NPs	Pb^{2+}	fluorescence quenching	0.51 nM	76
			fluorescence enhancement	1.5 nM	83
		Hg^{2+}	fluorescence enhancement	0.32 μM	80
				30 nM	88
			NSET	2 nM	92
		Zn^{2+}	fluorescence enhancement	0.76 μM	81
		Cu^{2+}	FRET	0.3 nM	82
				9.83 pM	87
		K^{+}	FRET	100 μM	90
		Tb^{3+}	FRET	N. A.	93
	Metal NCs	Hg^{2+}	fluorescence quenching	0.5 nM	114
		Cu^{2+}	fluorescence quenching	5 nM	110
		Pb^{2+}	fluorescence quenching	2 nM	126
		Fe^{3+}	AIFQ	3.5 μM	132
Upconversion nanoparticles		Hg^{2+}	LRET	0.06 nM	156
				41 nM	158
		Pb^{2+}	FRET	80 nM	161
			fluorescence enhancement	20 nM	162
		Cu^{2+}	FRET	1 μM	166
Semiconductor nanoparticles	Undoped QDs	Cu^{2+}	fluorescence quenching	7.1 nM	195
			fluorescence enhancement	2.75 nM	220
		Pb^{2+}	fluorescence enhancement	0.2 nM	216
		Ca^{2+}	FRET	2 μM	219
	Doped QDs	Hg^{2+}	fluorescence enhancement	0.18 nM	232
		Ag^{+}	NSET	7.9 nM	233
		Fe^{2+}	fluorescence quenching	3 nM	234
Carbon Materials	CDs	Hg^{2+}	fluorescence enhancement	20 nM	246
			fluorescence quenching	0.1 μM	247
	GQDs	Cu^{2+}	fluorescence quenching	282.9 nM	255
		Cr6+	fluorescence quenching	40 nM	257
	CNTs	Ag+	fluorescence enhancement	1 nM	268
		Hg^{2+}	FRET	15 nM	264
		Ag+		18 nM	
		Pb^{2+}		20 nM	
	Graphene	Hg^{2+}	fluorescence enhancement	0.92 nM	261

Author Manuscript

Author Manuscript

Author Manuscript

Author Manuscript

Type of nanomaterials[a]		Analytes	Detection mechanism[a]	Detection limit	Reference
		Ag+	FRET	20 nM	279
		Hg^{2+}		5.7 nM	

[a]NPs: nanoparticles; NCs: nanoclusters; CDs: carbon dots; GQDs: graphene quantum dots; CNTs: carbon nanotubes; NSET: nanometal surface energy transfer; FRET: fluorescence resonance energy transfer; N. A.: Not available; AIFQ: aggregation-induced fluorescence quenching; LRET: luminescence resonance energy transfer